HAL
open science

Subcellular specificity of cannabinoid effects in striatonigral circuits

Edgar Soria-Gomez, Antonio Pagano Zottola, Yamuna Mariani, Tifany Desprez, Massimo Barresi, Itziar Bonilla-del Río, Carolina Muguruza, Morgane Le Bon-Jego, Francisca Julio-Kalajzić, Robyn Flynn, et al.

To cite this version:

Edgar Soria-Gomez, Antonio Pagano Zottola, Yamuna Mariani, Tifany Desprez, Massimo Barresi, et al.. Subcellular specificity of cannabinoid effects in striatonigral circuits. Neuron, 2021, 109 (9), pp.1513-1526.e11. 10.1016/j.neuron.2021.03.007 . hal-03375577

HAL Id: hal-03375577

https://hal.science/hal-03375577

Submitted on 15 Oct 2021

HAL is a multi-disciplinary open access archive for the deposit and dissemination of scientific research documents, whether they are published or not. The documents may come from teaching and research institutions in France or abroad, or from public or private research centers.

L'archive ouverte pluridisciplinaire **HAL**, est destinée au dépôt et à la diffusion de documents scientifiques de niveau recherche, publiés ou non, émanant des établissements d'enseignement et de recherche français ou étrangers, des laboratoires publics ou privés.

SUBCELLULAR SPECIFICITY OF CANNABINOID EFFECTS IN STRIATONIGRAL CIRCUITS

Edgar Soria-Gomez[1,2,3,4,5,15,16*], Antonio C. Pagano Zottola[1,2,15], Yamuna Mariani[1,2,15], Tifany Desprez[1,2], Massimo Barresi[2,6], Itziar Bonilla-del-Río[3,4], Carolina Muguruza[7], Morgane Le Bon-Jego[2,6], Francisca Julio-Kalajzić[1,2], Robyn Flynn[8,9], Geoffrey Terral[1,2], Ignacio Fernández-Moncada[1,2], Laurie M. Robin[1,2], Jose F. Olivera da Cruz[1,2], Simone Corinti[1,2], Yasmine Ould Amer[10], Julia Goncalves[1,2], Marjorie Varilh[1,2], Astrid Cannich[1,2], Bastien Redon[1,2], Zhe Zhao[1,2], Thierry Lesté-Lasserre[1,2], Peggy Vincent[1,2], Tarson Tolentino-Cortes[11], Arnau Busquets-García[1,2], Nagore Puente[3,4], Jaideep S. Bains[9], Etienne Hebert-Chatelain[10], Gabriel Barreda-Gómez[11], Francis Chaouloff[1,2], Alexander W. Lohman[8,9,12], Luis F. Callado[7,13], Pedro Grandes[3,4,14], Jerome Baufreton[2,6], Giovanni Marsicano[1,2,16,17*], Luigi Bellocchio[1,2,16*]

[1]INSERM, U1215 NeuroCentre Magendie, Endocannabinoids and Neuroadaptation, Bordeaux, France; [2]University of Bordeaux; [3]Dept. of Neurosciences, Faculty of Medicine and Nursing, University of the Basque Country UPV/EHU, Leioa, Spain; [4]Achucarro Basque Center for Neuroscience, Leioa, Spain; [5]IKERBASQUE, Basque Foundation for Science; [6]IMN-UMR CNRS 5293 Neurodegenerative Diseases Institute, Bordeaux, France; [7]Dept. of Pharmacology, University of the Basque Country UPV/EHU, Leioa, and Centro de Investigación Biomédica en Red de Salud Mental (CIBERSAM), Spain. [8]Department of Cell Biology and Anatomy, Cumming School of Medicine, University of Calgary, Calgary, AB Canada; [9]Hotchkiss Brain Institute, University of Calgary, Calgary, AB Canada; [10]Canada Research Chair in Mitochondrial Signaling and Physiopathology, Department of Biology, University of Moncton, NB Canada; [11]Department of Research and Development, IMG Pharma Biotech S.L., Derio, Spain; [12]Alberta Children's Hospital Research Institute, University of Calgary, Calgary, AB Canada; [13]Biocruces Bizkaia Health Research Institute, Barakaldo, Spain; [14]Division of Medical Sciences, University of Victoria, Victoria, BC, Canada.

[15] These authors contributed equally

[16] Senior Authors

[17] Lead Contact

*Correspondence to: Edgar Soria-Gomez, edgar.soria@achucarro.org
Luigi Bellocchio, luigi.bellocchio@inserm.fr
Giovanni Marsicano, giovanni.marsicano@inserm.fr

SUMMARY

Recent advances in neuroscience positioned brain circuits as the key units controlling behavior, implying that their positive or negative modulation necessarily leads to specific behavioral outcomes. However, emerging evidence suggests that activation or inhibition of specific brain circuits can actually produce multimodal behavioral outcomes. Here we show that, in the same neuronal circuit, activation of a receptor at different subcellular locations can determine distinct specific behaviors. Pharmacological activation of type-1 cannabinoid receptors (CB_1) in the striatonigral circuit elicits both antinociception and catalepsy in mice. The reduction of nociception depends on the activation of plasma membrane-residing CB_1 receptors ($pmCB_1$), leading to inhibition of PKA activity and Substance-P release. Conversely, mitochondrial-associated CB_1 receptors ($mtCB_1$) located at the same terminals mediate cannabinoid-induced catalepsy through decrease of intra-mitochondrial PKA-dependent cellular respiration and synaptic transmission. Thus, subcellular-specific CB_1 receptor signaling within striatonigral circuits determines multimodal control of behavior.

KEYWORDS: CB_1 receptor, catalepsy, antinociception, THC, mitochondria, substantia nigra, PKA, Substance-P.

INTRODUCTION

The cannabinoid receptor type-1 (CB_1) is the main target of cannabinoid compounds. Cannabinoids possess high therapeutic potentials (Cohen et al., 2019), particularly in the management of pain sensitivity (Donvito et al., 2018). However, because of significant side-effects (e.g., cognitive and motor dysfunctions; Borgelt et al., 2013; Prashad and Filbey, 2017) their medical and recreational use is under intense scrutiny (Cohen et al., 2019). In particular, activation of CB_1 receptors impairs motor control (Giuffrida and Seillier, 2012; Monory et al., 2007) and cataleptic-like effects are considered the leading cause of vehicle accidents caused by human cannabis consumption (Martin et al., 2017).

Basal ganglia circuits, classically associated with motor control, are now studied in different contexts, including cognition and nociception. In particular, striatonigral circuits formed by dopamine receptor type-1 (D_1)-positive striatal medium spiny neurons projecting to the substantia nigra pars reticulata (SNr) play crucial roles in motor regulation (Freeze et al., 2013) and participate in nociception (Taylor et al., 2016). Indeed the SNr represents the ideal hub coordinating voluntary movement and nociceptive responses according to the different inputs received (Zhou et al., 2016), and displays one of the highest levels of CB_1 receptor protein expression in the brain (Marsicano and Kuner, 2008).

Neuronal CB_1 receptors are predominantly associated with presynaptic terminal plasma membranes ($pmCB_1$; Ibsen et al., 2017) and their activation mainly

results in the fine-tuned regulation of neurotransmitter and neuropeptide release (Busquets-Garcia et al., 2018). However, recent data indicate that functional CB_1 receptors are also present in intracellular compartments, particularly in association with mitochondria ($mtCB_1$; Benard et al., 2010; Busquets-Garcia et al., 2018; Hebert-Chatelain et al., 2016; Jimenez-Blasco et al., 2020; Koch et al., 2015), where they modulate bioenergetic and memory processes (Hebert-Chatelain et al., 2016). Indeed, normal mitochondrial functions are required for proper synaptic transmission underlying behavioral control (Francisco et al., 2020; Kanellopoulos et al., 2020; Rangaraju et al., 2014).

The double subcellular functional localization of CB_1 receptors in striatonigral circuits suggests that cannabinoids might exert different effects not only by altering the functions of different cell types and brain circuits, but also by impacting different subcellular processes within the same circuits. Thus, here we used the diverse distribution of CB_1 receptors as a tool to investigate whether subcellular constraints in the same neuronal circuit can determine multimodal behavioral control.

RESULTS

Striatonigral CB_1 receptors mediate cannabinoid-induced motor impairments and antinociception

Cannabinoid agonists dose-dependently decrease motor activity and induce antinociception through the activation of central CB_1 receptors (Metna-Laurent et al., 2017; Monory et al., 2007). To test whether CB_1 receptor signaling in the SNr is responsible for these effects, we locally infused (**Figure S1A**) the CB_1

receptor-selective antagonist AM251 in mice systemically treated (intraperitoneal, i.p.) with the plant-derived CB_1 receptor agonist Δ^9-tetrahydrocannabinol (THC, 10 mg/kg). AM251 fully blocked the THC-induced reduction in locomotor activity in the open field (**Figure S1B**), catalepsy in the horizontal-bar test (**Figure 1A**) and antinociception in the hot-plate test (**Figure 1B**), indicating that activation of CB_1 receptors in this brain region is necessary for these effects. As a control, voluntary or accidental misplacement of the cannulas to brain areas just adjacent to the SNr (**Figure S1A**) eliminated any impact of AM251 on THC-induced catalepsy, antinociception or hypolocomotion (**Figure 1A, 1B and S1B**), clearly indicating the local specificity of the effect.

The SNr receives direct (striatonigral) and indirect (striatopallidal - pallidonigral) information from striatal medium spiny neurons (MSNs). MSNs belonging to the direct pathway preferentially express dopamine D_1R receptor, whereas the indirect pathway ones are identified by the expression of dopamine D_2R receptor, although in the external segment of the Glubus Pallidus (GPe) there are some collateral D_1R-positive projections (Freeze et al., 2013). Interestingly, CB_1 receptors are abundantly expressed by both neuronal populations (Fernandez-Ruiz et al., 2011). To identify which subpopulation of CB_1 receptors are responsible for the antinociceptive and motor effects of THC, we used an intersectional recombinase approach (Zhao et al., 2020). We injected a recombinant adeno-associated virus (rAAV) expressing the Cre recombinase protein in a flipase (FLP)-dependent manner (AAV-FRT-iCre-EGFP) in the striatum of mice carrying a “floxed” CB_1 gene (*CB_1*-flox; Marsicano et al., 2003). Simultaneously, a retrograde rAAV expressing flipase (AAV-retro-FLP-BLFP)

was administered into either the GPe or the SNr (**Figure S1C**). Thus, we obtained the expression of the Cre recombinase in striatopallidal or striatonigral neurons of *CB_1*-flox mice, leading to the generation of ST-GP-*CB_1*-KO or ST-SN-*CB_1*-KO mutants that carrying the deletion of the receptor gene in either populations, respectively (**Figure S1C**). *In situ* hybridization coupled to GFP immunostaining for Cre detection showed that the recombinase was preferentially expressed in D_1R neurons over D_2R in ST-SN-*CB_1*-KO (D_1R/Cre cells 68.5±2.8%; D_2R/Cre cells 9±1%) with an opposite situation in ST-GP-*CB_1*-KO (D_1R/Cre cells 21.7±1.9%; D_2R/Cre cells 42.5±5.1%).

Deletion of CB_1 receptor gene in these models was confirmed by double *in situ* hybridization experiments, which showed preferential loss of CB_1 receptor expression by D_1R-expressing striatal neurons in ST-SN-*CB_1*-KO mice and by D_2R expressing neurons in the ST-GP-*CB_1*-KO mice (**Figure S1D**). Accordingly, ST-SN-*CB_1*-KO showed a consistent reduction of CB_1 immunoreactivity in the SNr whereas in ST-GP-*CB_1*-KO, CB_1 protein was selectively reduced in the GPe (**Figure 1C)**.

Whereas ST-GP-*CB_1*-KO mice responded to THC treatment similar to control animals, ST-SN-*CB_1*-KO littermates did not display either catalepsy or antinociception upon THC administration (**Figure 1D and 1E**). On the other hand, the hypolocomotor effect of THC was maintained upon both manipulations (**Figure S1E**), suggesting that other subpopulations of SNr CB_1 receptors are likely involved in this effect. These data indicate that activation of CB_1 receptors expressed at striatonigral, but not striatopallidal, terminals is

necessary for THC-induced antinociception and catalepsy, revealing a common anatomical target for these effects.

Cannabinoid-induced antinociception relies on activation of striatonigral pmCB_1 and regulation of Substance-P/NK_1 receptor activity

THC and AM251 are lipophilic molecules, which easily cross biological membranes, thereby potentially acting at both plasma membrane and intracellular CB_1 receptors. To distinguish between the contributions of these two pools of CB_1 receptors to the THC effects in the SNr, we locally administered the CB_1 receptor antagonist Hemopressin (Hp; Heimann et al., 2007). Hp is a peptide compound, which is unable to cross the plasma membrane (Benard et al., 2012) and, thereby, antagonizes only pmCB_1 receptors but not intracellular ones (Benard et al., 2012; Rozenfeld and Devi, 2008). Intra-SNr administration of Hp did not exert any effect by itself and it was not able to reverse THC-induced catalepsy (**Figure 1F**), but it strongly reduced the antinociceptive effect of THC (**Figure 1G**). Striatonigral neurons are known to release several neuropeptides, including Substance-P (Deniau et al., 2007; Johnson et al., 2016), which promotes pain perception *via* central activation of its main target, the type-1 neurokinin receptor (NK_1; Steinhoff et al., 2014). Interestingly, inhibition of NK_1 signaling can decrease pain reactions induced by systemic CB_1 receptor blockade (Darmani and Pandya, 2000), and some evidence suggests a negative role of CB_1 receptor signaling in Substance-P

production and release in the spinal cord and the striatum (Lever and Malcangio, 2002; Steiner et al., 1999). To test whether Substance-P signaling in the SNr might underlie THC-induced antinociception, we systemically administered the selective NK_1 receptor agonist GR73632 (Ray et al., 2009), in combination with THC. GR73632 (75 µg/kg) alone had no effect in any test, and it did not alter the cataleptic effect of THC (**Figure S1F**). However, this treatment blocked the antinociceptive effect of the cannabinoid (**Figure S1G**). Then, in order to verify that the interaction between CB_1 and NK_1 receptors occurs in the SNr, GR73632 was locally injected before systemic THC treatment. This treatment did not alter THC-induced catalepsy (**Figure 1H**), but, strikingly, it fully abolished the antinociceptive effect of THC (**Figure 1I**). These data show that cannabinoid-induced antinociception involves Substance-P signaling, suggesting that activation of CB_1 receptors might reduce the release of the neuropeptide at striatonigral terminals. To test this hypothesis, we established an *ex vivo* “sniffer cells” approach (**Figure S1H**), which has been already successfully used to detect the release of other neuropeptides in real time (Zaelzer et al., 2018). We transfected HEK-293T cells with 2 plasmids for co-expression of NK_1 receptor together with the calcium indicator GCaMP6s (**Figure S1H**) to obtain cells capable of detecting exogenously applied Substance-P in a very sensitive (EC50, 5.1 nM) and specific way (**Figure S1H and S1I**). These cells were then seeded over acute sagittal brain slices containing the striatonigral pathway (**Figure 1J**). After 2-hour rest to allow cellular adhesion to the slices, GCaMP6s fluorescence was imaged (Zaelzer et al., 2018) (**Figure 1J**) before and after electrical stimulation of the striatonigral afferents. This manipulation elicited a marked increase in GCaMP6s

fluorescence in cells placed above the SNr (**Figure 1K, S1J, S1K, S1L, S1M**), indicating an increase in Substance-P release. The increase in fluorescence is specific for the peptide, since is absent when slices are treated with cells only expressing GCaMP6s (**Figure S1J and S1L**) and it was blocked by the NK_1 selective antagonist CP122721 (**Figure S1K and S1L**). Strikingly, application of the cannabinoid agonist WIN55,212-2 (WIN) dramatically reduced electrically evoked Substance-P release in wild type mice (**Figure 1K and S1M**), but not in *CB_1*-KO littermates (**Figure 1K**). WIN did not affect the response to exogenous peptide (**Figure S1N**), showing that its effect in slices was due to a CB_1 receptor-mediated decrease of Substance-P release.

To further confirm the striatonigral origin of Substance-P release as well as its modulation by cannabinoids, we coupled the sniffer cells approach to optogenetic stimulation (Zaelzer et al., 2018). For this aim, we virally expressed the red-activated channelrhodopsin ChrimsonR (Klapoetke et al., 2014) in D_1R-Cre positive cells (Lemberger et al., 2007) of the striatum and then we conducted sniffer experiments in SNr slices (**Figure 1L**). As technical validations of the approach, we also performed patch clamp experiments in SNr neurons upon light stimulations. As expected based on the partial spectrum overlapping of the used light wavelength (Klapoetke et al., 2014), the application of the blue light to record calcium levels in the sniffer cells induced a slight activation of Chrimson and triggered-GABAergic currents which, however, had a much lower amplitude than the ones triggered by the red light (**Figure S1O**). Thus, some experiments had to be discarded because the blue-light stimulation was able to saturate the subsequent red-light-induced Substance-P

release. Nevertheless, Chrimson activation by red-light triggered above-baseline calcium responses in sniffer cells in approximately 50% of the experiments. In these conditions, calcium responses indicating Substance-P release were drastically reduced by the application of WIN (**Figure 1M**), similarly as previously observed with electrical stimulation.

Altogether, these data indicate that pmCB_1 receptors at D_1R-positive striatonigral terminals are responsible for THC-induced antinociception, involving the modulation of Substance-P/NK_1 signaling. Additionally, these results point out a different mechanism for the cataleptic effect, which likely involves intracellular CB_1 receptors in the SNr.

Subcellular localization of CB_1 receptors in the SNr

To investigate the intracellular distribution of the CB_1 receptor in the SNr, we used immunogold electron microscopy (Puente, 2019). The majority of CB_1 receptor protein in the SNr of WT mice was associated to the plasma membrane (pmCB_1) of synaptic terminals (**Figure 2A-C and S2A**). Quantifications of gold particles using stringent parameters to identify mitochondrial-localized immunoreactivity (Puente, 2019) revealed that CB_1 receptors in the SNr are anatomically associated to mitochondrial membranes (mtCB_1) with a density of approximately 3 particles per 20 μm^2 (**Figure 2A-D and S2A**). Moreover, approximately 10% of total mitochondria analyzed were labeled with CB_1 receptor in WT mice (**Figure 2A-E and S2A**). Conversely, only background levels of CB_1 immunoreactivity was detected in any analyzed compartment of *CB_1*-KO mice (**Figure 2A-E and S2A**), clearly demonstrating the existence of mtCB_1 in striatonigral terminals.

Generation of DN22-*CB_1*-KI mutant mice, lacking mtCB_1 receptors

We previously showed that a mutant version of the CB_1 protein lacking the first 22 amino acids (called DN22-CB_1) is neither anatomically nor functionally associated to mitochondrial membranes, nevertheless maintaining its other functions (e.g. at plasma membrane; Hebert-Chatelain et al., 2016). Thus, we generated a new knock-in mutant mouse line (called DN22-*CB_1*-KI; Pagano Zottola et al., 2020), in which the wild-type *CB_1* receptor gene is replaced by the coding sequence of the DN22-CB_1 protein (**Figure S2B**). Quantifications of CB_1 receptor mRNA (by qRT-PCR) and protein (by immunofluorescence) revealed no significant differences between WT and DN22-*CB_1*-KI mice in many different brain regions (**Figure S2C and S2D**). Counting of gold particles in immuno-electron microscopy experiments indicated that the total amount of CB_1 receptor protein in the SNr was not significantly different between DN22-*CB_1*-KI and WT littermates (**Figure 2F, 2G and S2D**). Similarly, the levels of pmCB_1 were not impacted by the mutation (**Figure 2F, 2H and S2D**). However, the density of mitochondrial-associated mtCB_1 receptors and the percentage of CB_1-positive mitochondria were significantly lower in DN22-*CB_1*-KI mice as compared to WT littermates, reaching levels undistinguishable from global *CB_1*-KO mice (**Figure 2F, 2I, 2J and S2D**). To test the ability of DN22-CB_1 receptors to activate G protein signaling, we performed [^{35}S]GTPγ binding assays upon stimulation with the cannabinoid agonist WIN in cortical, hippocampal and midbrain extracts from WT, *CB_1*-KO, and DN22-*CB_1*-KI mice (**Figure 2K**). The DN22-CB_1 mutant was as efficient as its wild-type cognate in triggering G protein activation (**Figure 2K**). These results were also confirmed by *in situ* [^{35}S]GTPγ binding assays in other brain regions (**Figure S2E and S2F**). Moreover,

autoradiographic analyses of [^{3H}]CP55.940 cannabinoid agonist binding in parallel sections did not identify any significant difference between the two genotypes (**Figure S2G and S2H**). Thus, DN22-*CB_1*-KI mice display normal binding of cannabinoid ligands and subsequent activation of G-protein signaling.

Oxygen consumption assays in substantia nigra (SN) homogenates revealed that WIN lowered ADP-stimulated mitochondrial respiration in WT but not in *CB_1*-KO mice (**Figure 2L and S2I**), indicating a specific CB_1-mediated control of mitochondrial activity. Notably, this effect was also abolished in SN homogenates from DN22-*CB_1*-KI mice, showing its dependency on mtCB_1 receptors (**Figure 2L and S2I**). The DN22-*CB_1*-KI mutant strain was viable, fertile and presented normal body weight, muscular strength and locomotion (**Figure S3A and S3B**). Interestingly, DN22-*CB_1*-KI mice did not display any alteration in voluntary running wheel activity (**Figure S3C**), where global *CB_1*-KO mice are impaired (Dubreucq et al., 2010), showing that certain CB_1 receptor-dependent behavioral functions are maintained in these mutants. Previous evidence suggests that mtCB_1 receptors might be partly responsible for electrophysiological depolarization-induced suppression of inhibition in the hippocampus (DSI; Benard et al., 2012), which is known to depend on endocannabinoid signaling (Wilson et al., 2001). Interestingly, DN22-*CB_1*-KI mice displayed DSI, but its amplitude was slightly decreased as compared to WT littermates (**Figure S3D and S3E**), confirming the participation of mtCB_1 receptors in this form of synaptic plasticity (Benard et al., 2012). Altogether, these observations indicate that the constitutive deletion of the first 22 amino

acids of the CB_1 protein specifically impacts the effects of cannabinoids involving mitochondrial activity, but leave other functions of CB_1 receptors unchanged. Therefore, DN22-*CB_1*-KI mutant mice represent a novel and suitable tool to untangle the roles of $mtCB_1$ receptors.

Activation of $mtCB_1$ receptors decreases synaptic transmission at striatonigral terminals and induces catalepsy, but not antinociception

To explore if $mtCB_1$ receptors participate in the well-known cannabinoid control of synaptic transmission in the SNr (Sales-Carbonell et al., 2013; Szabo et al., 2000), we performed optogenetic-coupled electrophysiological recordings of striatonigral neurotransmission in slices. The rAAV expressing channelrhodopsin (Chr2) under the neuronal synapsin promoter (AAV-synP-Chr2-mCherry) was injected into the dorsal striatum (**Figure 3A**) of DN22-*CB_1*-KI, *CB_1*-KO mice and WT littermates. Non-dopaminergic neurons receiving Chr2-expressing fibers from striatonigral projecting neurons were recorded using whole-cell patch clamp in SNr slices (**Figure 3B**). Delivery of brief light-pulses on striatonigral terminals triggered reliable optically-induced inhibitory post-synaptic currents (oIPSCs) in SNr neurons, which were sensitive to $GABA_A$ blockade (**Figure 3C**). Treatment with WIN (5 µM) reduced oIPSCs in WT but not in *CB_1*-KO mice (**Figure 3D and 3E**), suggesting a CB_1-dependendent mechanism. Interestingly, WIN-mediated reduction of oIPSCs was absent in slices from DN22-*CB_1*-KI mice (**Figure 3D and 3E**). Furthermore, no changes

were observed in the paired-pulse ratio during baseline, indicating a normal synaptic efficiency in DN22-*CB_1*-KI mice as compared to their WT littermates (**Figure S3F**). These data indicate that mtCB_1 receptors are necessary for the cannabinoid-induced inhibition of synaptic transmission in the striatonigral pathway, which has been proposed as a potential mechanism for cannabinoid-induced catalepsy (Garcia et al., 2016). Accordingly, THC or WIN administrations induced strong catalepsy in WT mice, but not in DN22-*CB_1*-KI littermates (**Figure 3F**). Conversely, both genotypes displayed normal cannabinoid-induced antinociception (**Figure 3G**). Interestingly, WIN application reduced Substance-P release in DN22-*CB_1*-KI SNr slices (**Figure S3G**) to a similar extent as observed in WT slices (**Figure 1K**). Furthermore, both intra-SNr hemopressin infusion (**Figure S3H**), as well as systemic administration of the NK_1 receptor agonist GR73632 (**Figure S3I**) strongly reduced THC-induced antinociception in DN22-*CB_1*-KI mice. Therefore, the CB_1-dependent control of Substance-P release in the SNr, and subsequent antinociceptive effect, do not require mtCB_1 receptors. These data show that the activation of mtCB_1 receptors is necessary for cannabinoid-induced synaptic depression in the SNr and catalepsy. Conversely, mtCB_1 receptors are dispensable for the local cannabinoid-induced signaling leading to antinociception. Thus, a mechanistic double dissociation of these effects of cannabinoids seems to exist in the SNr.

Cannabinoid-induced catalepsy relies on activation of striatonigral mtCB_1 receptors and mitochondrial inhibition

Striatal dopamine receptor type-1 (D_1)-positive cells are one of the major components of striatonigral circuits (Freeze et al., 2013). Notably, mice lacking the *CB_1* gene in D_1-positive cells (D_1-*CB_1*-KO) do not display cannabinoid-induced catalepsy (Monory et al., 2007). We took advantage of this phenotype to investigate the specific impact of striatonigral mtCB_1 receptor activation on the cataleptic effect of cannabinoids. For this purpose, we adopted a CB_1 rescue approach (**Figure 4A**) by injecting Cre-dependent viral vectors expressing CB_1 or DN22-CB_1 (AAV-DIO-CB_1 or AAV-DIO-DN22-CB_1, respectively) directly into the dorsal striatum of D_1-*CB_1*-KO mice (expressing Cre specifically in D_1 positive cells) to specifically target striatonigral neurons (**Figure 4B and 4C**). Oxygen consumption assays revealed that WIN failed to decrease mitochondrial respiration in SN extracts from D_1-*CB_1*-KO mice injected with a control virus (**Figure 4D**). The re-expression of CB_1 receptors in striatal D_1-positive cells of mutant mice fully rescued the cannabinoid-induced decrease of oxygen consumption in the SN (**Figure 4D**), whereas the injection of AAV-DIO-DN22-CB_1 was not able to restore this effect (**Figure 4D**). The rescue of CB_1 receptors in striatonigral cells was sufficient to restore the cataleptic effect of THC in D_1-*CB_1*-KO mice (**Figure 4E**). In contrast, no catalepsy was observed after DN22-CB_1 expression in THC-treated D_1-*CB_1*-KO mice (**Figure 4E**). Additionally, we performed correlation analysis between the levels of CB_1 expression (**Figure 4C**) and THC-induced catalepsy (**Figure 4E**) in mice with rescue of CB_1 or DN22-CB_1. The absence of positive correlation

(**Figure S3J**) between the parameters, indicates that the subcellular localization rather than the expression levels of CB_1 determines the cataleptic effect of cannabinoids.

Thus, $mtCB_1$ receptor signaling in the striatonigral circuit is responsible for the local reduction of mitochondrial respiration and the cataleptic effect induced by cannabinoids.

Cannabinoid-induced catalepsy involves striatonigral mitochondrial sAC activity

To identify the molecular machinery linking the effects of cannabinoids on SN mitochondrial respiration and catalepsy, we aimed at dissecting the intramitochondrial signaling pathways involved. Stimulation of $mtCB_1$ receptors activates intra-mitochondrial $G\alpha_i$ proteins, thereby inhibiting soluble adenylyl cyclase (sAC) and protein kinase-A (PKA) activities (Hebert-Chatelain et al., 2016). The cannabinoid-induced reduction of mitochondrial respiration in SN extracts was abolished by pretreatment with the sAC inhibitor KH7 (**Figure 4F**), suggesting that sAC activity is involved in $mtCB_1$ receptor-dependent effects in this brain region. On the other hand, pre-treatment with the NK_1R agonist GR73632 did not impact the effect of WIN on SN respiration (**Figure S3K**), suggesting dissociation between the two pathways. To investigate whether the intra-mitochondrial sAC pathway participates in the SNr-dependent behavioral effects of THC, we first locally injected KH7 before systemic THC treatment. The sAC inhibitor blocked the cataleptic effect of THC (**Figure 4G**), without

impacting the behavior of mice in the hot-plate test (**Figure 4H**). Thus, similarly to the impact on mitochondrial respiration, the cataleptic effect of THC requires sAC activity in the SNr. However, these results do not show that the CB_1 signaling involved in catalepsy is specific of striatonigral neurons. Since sAC expression is not limited to mitochondria and KH7 can have additional targets (Valsecchi et al., 2014), pharmacological experiments cannot provide definitive information about the subcellular location and the molecular specificity of the observed effects. To address these issues, we used a Cre-dependent viral approach to overexpress a mitochondrial-targeted version of sAC (mt-sAC-HA; Hebert-Chatelain et al., 2016; Valsecchi et al., 2014) that was previously reported to be targeted to mitochondria (**Figure S3L**, Pearson's coefficient 0.70±0.04; Hebert-Chatelain et al., 2016) and block respiratory effects of cannabinoids in cell cultures (Hebert-Chatelain et al., 2016). Striatonigral overexpression of mt-sAC obtained by injecting AAV-DIO-mt-sAC-HA into the dorsal striatum of D_1-Cre mice (Lemberger et al., 2007) (**Figure S3M and N**) fully blocked the cannabinoid effect on mitochondrial respiration in SN extracts (**Figure 4I and S3O**). Strikingly, these mice did not present any cataleptic effect upon THC administration as compared to control mice (**Figure 4J**), whereas they displayed a normal THC-induced antinociception (**Figure 4K**). These data show that inhibition of intra-mitochondrial sAC signaling in striatonigral terminals is not involved in antinociception, but it underlies the cannabinoid-induced decrease of mitochondrial respiration and the subsequent cataleptic effect.

PKA signaling mediates both cannabinoid-induced catalepsy and antinociception, but in different subcellular compartments

Adenylyl cyclase activity triggers several signaling pathways and the activation of PKA is one of the most prominent (Dwivedi and Pandey, 2008). Inhibition of PKA is one of the best characterized signaling mechanisms of CB_1 receptor activation throughout the brain (Ibsen et al., 2017), including in striatal neurons (Borgkvist and Fisone, 2007; Martinez et al., 2012). For instance, the activity of this kinase is necessary for the stimulation of Substance-P release in spinal cord and cultured dorsal root ganglion neurons, and this mechanism is modulated by CB_1 receptors (Chen et al., 2018; Oshita et al., 2005). Within mitochondria, PKA signaling following mt-sAC activation is a target for $mtCB_1$-induced reduction of mitochondrial functions (Hebert-Chatelain et al., 2016). Thus, PKA inhibition at different subcellular locations might mediate $pmCB_1$-dependent antinociception and $mtCB_1$-dependent catalepsy, by reducing Substance-P release and inhibiting mitochondrial respiration, respectively. To test this hypothesis, we used constructs expressing constitutively active mutant forms of PKA (Niswender et al., 2005) targeted either to the cytosol (PKA-CA, myc tagged) or to the mitochondria (MLS-PKA-CA, myc-tagged, **Figure S3P**; Hebert-Chatelain et al., 2016). These constructs were used to generate rAAVs for Cre-dependent expression, which were injected into the dorsal striatum of D_1-Cre mice. By this way, we obtained expression of these two different forms of constitutively active PKA in striatonigral neurons (**Figure S3Q**). Expression of PKA-CA did not alter catalepsy, but it blocked the antinociceptive effect of THC (**Figure 4L and 4M**). Conversely, the expression of MLS-PKA-CA dampened

the cataleptic effect of THC, without changing the antinociception (**Figure 4L and 4M**). Importantly, the expression of PKA-CA did not alter cannabinoid-induced decrease of mitochondrial respiration in SN extracts, whereas MLS-PKA-CA abolished this effect (**Figure 4N and S3R**). These data show that inhibition of PKA activity in striatonigral neurons mediates both cataleptic and antinociceptive effects of cannabinoids. However, the specific subcellular location of the activity of this kinase is differentially involved in these effects. Whereas intra-mitochondrial sAC-PKA signaling mediates cannabinoid-induced decrease of mitochondrial respiration and catalepsy, the antinociceptive effect of these drugs relies on the inhibition of cytoplasmic PKA.

DISCUSSION

This study reveals that the differential subcellular localization of a receptor can bias the behavioral consequences of its activation in the same brain circuit. *Via* the regulation of specific subcellular molecular pathways, striatonigral neurons are the substrate of both adverse cataleptic and clinically-relevant antinociceptive effects of cannabinoids. While stimulation of $pmCB_1$ receptors at striatonigral terminals induces inhibition of nociceptive responses, presynaptic $mtCB_1$ receptors in the same location are responsible for cataleptic effects of cannabinoids (**Figure S4**). Mechanistically, cannabinoid-induced catalepsy relies on $mtCB_1$ receptor-dependent regulation of intramitochondrial sAC/PKA signaling, inhibition of mitochondrial respiration and decrease of inhibitory synaptic transmission at striatonigral terminals. Conversely, antinociception requires $pmCB_1$ receptor-dependent reduction of cytosolic PKA activity and decrease of Substance-P/NK_1 receptor signaling (**Figure S4**).

The SNr, being a key part of the basal ganglia loop (Freeze et al., 2013), is classically considered to provide mainly motor regulation, integrating striatal pathways and regulating the activity of motor cortex through thalamic projections (Borsook et al., 2010). However, the SNr also, directly and indirectly, modulates the activity of several brain regions involved in pain processing such as the superior and inferior colliculus, pedunculopontine nucleus (PPN), rostral ventral medulla and dorsal root ganglia (Borzook et al., 2010; Zhou, 2016). Moreover, several electrical and optogenetic stimulation studies revealed a novel nociceptive network, e.g Subthalamic Nucleus – SNr – superior colliculus and parabrachial nucleus (Luan et al., 2020; Pautrat et al., 2018). Thus, the SNr is ideally placed to control voluntary movement, as wells as nociceptive responses. There could be two different sets of striatonigral neurons, one dedicated to nociception control (as indicated by the presence of different nociceptive neurons in the SNr and the other to movement control (as already extensively studied (Borzook et al., 2010). Alternatively the same neurons could be involved in both effects according to the different inputs received and possibly differential molecular mechanisms triggered by those inputs (Chudler and Dong, 1995). In this scenario, the subcellular localization of CB_1 receptors could serve as a molecular switch regulating motor control and pain perception.

More recently, an emerging idea started to grow in brain research about the possibility that specific subcellular locations of a molecular process could trigger different cellular effects (Creighton, 2011; Ilouz et al., 2017). For instance, although their relative impact on behavior has not been investigated so far, specific subcellular locations of targeted molecules have been proposed to

differentially modulate cellular processes in the same brain cells (Bucko et al., 2019; Qi et al., 2019; Skalhegg and Tasken, 2000). The recent evidence that certain GPCRs, including CB_1, can functionally localize to different organelles (Benard et al., 2012; Eichel and von Zastrow, 2018; Hebert-Chatelain et al., 2016; Lahuna and Jockers, 2018) indicates that they might be directly involved in these subcellular-specific signaling pathways and their behavioral consequences. Moreover, given the crucial role of proper GPCRs trafficking for their activity (Lobingier and von Zastrow, 2019), one might speculate that a transient mitochondrial passage might be a determinant of certain CB_1 functions at plasma membranes. Although not yet possible to be directly addressed experimentally, this interesting hypothesis might change the current view of receptor trafficking and will be for sure the subject of future studies.

The activation of $mtCB_1$ receptors in striatonigral terminals is responsible for the effects of cannabinoids on cellular respiration, synaptic transmission and behavioral catalepsy. A growing body of evidence highlights the importance of mitochondrial functions for the regulation of synaptic transmission (Garcia et al., 2019; Vos et al., 2010), but little is known concerning the detailed molecular mechanisms linking the organelle to the synaptic machinery. The constant supply of ATP produced by mitochondria is considered to be a key element for sustaining synaptic transmission (Rangaraju et al., 2014). By regulating mitochondrial respiration at synaptic terminals, $mtCB_1$ receptors are therefore perfectly placed to potentially dampen inhibitory striatonigral neurotransmission and, thereby, induce catalepsy upon pharmacological activation. This suggests that similar mechanisms might occur during

physiological fine-tuned control of movements, thereby establishing a link between mitochondrial activity, synaptic transmission and motor control.

The assessment of nociception in animal models necessarily relies on the observation of motor responses. Thus, it has been proposed that cannabinoid-induced decrease of pain reactions might be secondary to motor impairments, such as catalepsy, rather than reflecting proper antinociception (Giuffrida and Seillier, 2012; Pertwee, 2001). However, analgesic and antinociceptive effects of cannabinoids have been observed at several supraspinal and spinal locations, in the absence of motor alterations, indicating that these two effects can be discriminated at the level of different brain and spinal cord regions (Woodhams et al., 2017). Our data show that both behavioral outputs can be mediated by activation of CB_1 receptors located in different subcellular organelles in striatonigral neurons, triggering distinct molecular mechanisms. This does not only add a new location for cannabinoid effects, but it also shows that CB_1 receptor-dependent catalepsy and antinociception rely on a true intracellular mechanistic dichotomy, likely involved in the physiological regulation of complex processes, such as motor and pain control. This dichotomy, observed after acute pharmacological activation of CB_1 receptor, might be also underlying the physiological role of endogenous cannabinoids in motor regulation and pain processing. Indeed, pharmacological and/or genetic CB_1 receptor blockade increases the sensitivity to pain perception (Clapper et al., 2010; Nadal et al., 2013) and also have been often reported to increase locomotor reactivity (Griebel et al., 2005; Häring et al., 2011). On the other hand, like THC and other cannabinoid agonists, inhibitors of endocannabinoids

degradation are able to induce antinociception and catalepsy via CB_1 receptor activation (Long et al., 2009), further confirming the endogenous role of the receptor in regulating these two physiological processes.

Cannabinoids induce antinociception through the $pmCB_1$ receptor-dependent reduction of Substance-P release in striatonigral neurons and the consequent decrease of local NK_1 receptor signaling. Interestingly, Substance-P in the SNr participates in pain processing, possibly through the modulation of the activity of rostral ventral medulla and dorsal root ganglia(Boccella et al., 2020; Borsook et al., 2010; Taylor et al., 2016). Therefore, the CB_1 receptor-dependent modulation of Substance-P/NK_1 signaling in the striatonigral neurons is a novel mechanism that likely participates in larger circuits modulating nociceptive responses.

To conclude, CB_1 receptors in the striatonigral circuit mediate cannabinoid-induced catalepsy and antinociception. This regulation clearly involves distinct subcellular and molecular mechanisms in the same neuronal circuit, resulting in the respective control of neurotransmitter and neuropeptide release. Thus, selective subcellular manipulations of CB_1 receptors represent a potential therapeutic strategy to avoid undesirable effects of cannabinoid drugs, and to promote their beneficial pain treatment. The unforeseen dichotomy between cannabinoid-induced mitochondrial catalepsy and non-mitochondrial antinociception in the same cellular population introduces the concept of subcellular specificity of behavioral control.

ACKNOWLEDGMENTS

We thank Delphine Gonzales, Nathalie Aubailly, and all the personnel of the Animal Facility of the NeuroCentre Magendie for mouse care. We also thank all the members of the Marsicano lab for useful discussions, Virginie Morales for invaluable help with administrative work. We thank the Histology and Biochemistry platforms of the NeuroCentre Magendie, as well as the Bordeaux Imaging Center (BIC) for help in the experiments. We thank G. Manfredi (Cornell University) for the mt-sAC–HA. We thank Su Melser for helpful suggestions regarding the mitochondrial respiration and Roman Serrat for help in imaging. We also thank Daniela Cota, Manuel Guzman, Pavel E. Rueda-Orozco, and Guillaume Ferreira for their useful and critical reading on the manuscript. This work was supported by INSERM (to G.M. and L.B.), EU–FP7 (PAINCAGE, HEALTH-603191 to G.M.), European Research Council (Endofood, ERC–2010–StG–260515; CannaPreg, ERC-2014-PoC-640923, Micabra to G.M.), Fondation pour la Recherche Medicale (DRM20101220445 to G.M. and ARF20140129235 to L.B.). Human Frontiers Science Program (to G.M.), Region Aquitaine (to G.M.), French State/Agence Nationale de la Recherche (LABEX BRAIN ANR-10-LABX-43 to G.M., JCJC MitoCB1-fat to L.B.), Marie Skłodowska-Curie Actions Individual Fellowships (H2020-MSCA-IF-2016, ID747487 to C.M.), the Basque Government (IT1211/19 to L.F.C.), Fyssen Foundation, CONACyT, Ikerbasque and MINECO (Ministerio de Economía y Competitividad) PGC2018-093990-A-I00 (MICIU/AEI/FEDER, UE) (to E.S.-G.). NSERC Discovery Grant - RGPIN-2019-06274 (to A.W.H. and R.F.). The Basque Government (IT1230-19 to P.G.), Red de Trastornos

Adictivos, Instituto de Salud Carlos III (ISC-III) and European Regional Development Funds-European Union (ERDF-EU; RD16/0017/0012 to P.G.), MINECO/FEDER, UE (SAF2015-65034-R to P.G.) and MINECO/FEDER, UE (POP contract BES-2016-076766 to I.B.-D.R.

AUTHOR CONTRIBUTIONS

E.S-G., and L.B., performed and analyzed behavioral, biochemical and anatomical experiments. A.C.P.Z., C.M., M.L.B-J., R.F., I.M.M., Y.O.A., A.C., T.L-L., P.V., T.T-C., J.S.B., E.H-C., G.B-G., A.W.L., and L.F.C. performed and analyzed biochemical experiments. Y.M., T.D., L.M.R., J.F.C.O., S.C., J.C., L.M., B.R., A.B-G., and F.C., performed and analyzed behavioral experiments. M.B., G.T., and J.B., performed and analyzed electrophysiological experiments. Y.M., I.B-d-R., M.V., Z.Z., F.J-K., N.P., and P.G., performed and analyzed anatomical experiments. E.S-G., G.M., and L.B., conceived and supervised the whole project and wrote the manuscript. All authors edited and approved the manuscript.

DECLARATION OF INTERESTS

The authors declare no competing interests.

STAR METHODS

Animals

Experiments were approved by the Committee on Animal Health and Care of INSERM, and the French Ministry of Agriculture and Forestry (authorization number 3306369). Mice were maintained under standard conditions (food and water *ad libitum*; 12h/12h light/dark cycle, light on 7 a.m.; experiments were performed between 9 a.m. and 5 p.m.). C57BL/6-N male mice (2–4 months old) were purchased from Janvier (France). D_1-CB_1-KO mice and their WTs littermates were generated and maintained as previously described(Monory et al., 2007). D_1-Cre mice(Lemberger et al., 2007) were kindly provided by Günther Schütz, (German Cancer Research Center). DN22-CB_1-KI mice were generated using a flox-stop strategy as previously described(Ruehle et al., 2013). Stop cassette was excised *via* a Cre deleter mouse strain and knock-in mice were maintained over a C57BL6/N background for several generations before experiments.

Drugs

THC was obtained from THC Pharm GmbH (Frankfurt, Germany). AM251, Hemopressin and GR73632 were purchased from Tocris (France). WIN 55,212-2 mesylate salt and KH7 were obtained from Sigma Aldrich (France). THC (10mg/kg) was dissolved in a mixture of saline (0.9% NaCl) with 5% ethanol and 4% cremophor. WIN 55,212-2 was dissolved in DMSO for *in vitro* experiments and in mixture of DMSO, Tween80 (1.25-1.25-97.5) and saline for *in vivo* treatments. Hemopressin (22 ng in 0.5 µl) and GR73632 (100ng in 0.5µl) were dissolved in saline. AM251 (4 µg in 0.5µl) and KH7 (2µg in 0.5µl) were

dissolved in 10% DMSO, 10% cremophor and 80% saline. Vehicles contained the same amounts of solvents respectively to the drug. All drugs were prepared fresh before the experiments.

Viral vectors

To generate AAV-DIO-CB_1, AAV-DIO-DN22, AAV-DIO-mt-sAC-HA, AAV-DIO-PKA-CA and AAV-DIO-MLS-PKA-CA the coding sequences for the 5 proteins(Hebert-Chatelain et al., 2016) were subcloned in pAAV-CAG-flex plasmid (kindly gifted by Matthias Klugmann, UNSW, Australia) by using standard molecular cloning techniques. The same pAAV-CAG-flex plasmid was used as empty control (AAV-DIO-ctr). AAVs were generated by PEI transfection of HEK 293T cells and purified by iodixanol-gradient ultracentrifugation as previously described(Hebert-Chatelain et al., 2016). Virus titers were $5.43*10^{11}$ for AAV-DIO-CB_1, $3.34*10^{11}$ for AAV-DIO-DN22, $2.36*10^{11}$ for AAV-DIO-mt-sAC-HA, $3.87*10^{11}$ for AAV-DIO-PKA-CA, $3.96*10^{11}$ for AAV-DIO-MLS-PKA-CA and $4.51*10^{11}$ for AAV-DIO-ctr, expressed as genomic copies (GC) x ml.

For optogenetic experiments, rAAV2-hSyn-ChR2(H134R)-mCherry (10^{13} GCxml) and rAAV-hSyn-DIO-ChrimsonR-tdTomato ($5.2*10^{12}$ GCxml) were purchased from UNC vector core (USA) and Viral Vector Facility (VVF) of the Neuroscience Center Zurich (Zentrum für Neurowissenschaften Zürich, ZNZ) respectively.

The viral vectors used for CB_1 deletion experiment (*see next section*) were purchased from the VVF. Titres were: $6.4*10^{12}$ for AAV-retro-hSyn1-EBFP2-FLPo, $4.1*10^{12}$ for AAV-retro-hSyn1-EBFP2 and $6.3*10^{12}$ for AAV-hEF1a-dFRT-iCre-EGFP.

Surgery and drug/virus administration

For intra-SNr injections of drugs mice were anesthetized by intraperitoneal injection of a mixture of ketamine (100mg/kg, Imalgene 500®, Merial) and Xylazine (10mg/kg, Rompun, Bayer) and placed into a stereotaxic apparatus (David Kopf Instruments) with mouse adapter and lateral ear bars. Mice were allowed to recover for at least one week in individual cages before the beginning of the experiments. Mice were weighed daily and individuals that failed to regain the pre-surgery body weight were excluded from the following experiments. Mice were bilaterally implanted with 3.5 mm stainless steel guide cannulae (Plastics One, USA) targeting the SNr with the following coordinates: AP -3.2, L ± 1.3, DV –3.5, according to Paxinos and Franklin(Paxinos and Franklin, 2001). Guide cannulae were secured with cement anchored to the skull by screws. The drug injections for intra-SNr were performed by using injectors protruding 1 mm from the tip of the cannula. The correct placement of the SNr cannulas was verified by injection of sky-blue toluidine followed by neutral red staining(Soria-Gomez et al., 2014) (**Figure S1A**).

AAV injections of AAV-DIO-CB_1 or AAV-DIO-DN22 in the dorsal striatum of D_1-*CB_1*-KO mice, or AAV-DIO-mt-sAC-HA, AAV-DIO-PKA-CA and AAV-DIO-MLS-PKA-CA in D_1-Cre mice, with respective AAV-DIO-Ctr, were performed with the following coordinates: AP +0,5 L ± 2,0, DV –3.0 as previously described(Bellocchio et al., 2016).

For the specific deletion of CB1 in the striatopallidal or striatonigral neurons, mice were anesthetized by inhalation of isofluorane 5% and placed into the stereotaxic apparatus with the anesthesia maintained at 2% during the entire

surgery. AAV vectors were injected with the help of a microinjector (Nanoject III, Drummond Scientific, PA, USA). The deletion was performed injecting the viral vectors AAV-hEF1a-dFRT-iCre-EGFP in the dorsal striatum, STR (2 injections of 1µl per side) with the following coordinates: AP + 0,8 ML ± 2,0 DV -3,0 and -3,5; and the retrogade vector AAV-retro-hSyn1-EBFP2-FLPo or AAV-retro-hSyn1-EBFP2 as control in one of its target external Globus Pallidus, GPe or Substantia nigra pars reticulata, SNr (respectively AP – 0,5 ML ± 1,8 DV – 4,25; volume 350 nl per side and AP – 3,25 ML ± 1,35 DV – 4,5; volume 750 nl per side).

Animals were allowed to recover for at least four weeks before the beginning of biochemical (see after) or behavioral experiments. Mice that underwent behavioral experiments were fixed by transcardial perfusion of 4% PFA and their brain were processed for imaging (to detect BFLP and EGFP) and double fluorescent in-situ hybridization (see below), or for immunofluorescence as previously described (Hebert-Chatelain et al., 2016), with primary antibodies directed against CB_1 receptor (CB_1-Go-Af450-1; 2 µg/ml; Frontier Science Co. Ltd), to detect CB_1 rescue and CB_1 deletion, or against HA-tag (#3724; Cell Signaling Technology Danvers, MA) to confirm overexpression of mt-sAC. Mice that did not fulfill histological positive criteria were excluded from the study.

Double fluorescent in-situ hybridization coupled to GFP immunodetection

Double FISH/GFP immunofluorescence experiments to measure the number of CB_1/D_1R vs CB_1/D_2R positive striatal neurons in the deletion experiments, were carried out as previously described (Oliveira da Cruz et al., 2020; Terral et al., 2019). Briefly, free-floating frozen coronal sections were cut out with a cryostat

(30 µm, Microm HM 500M Microm Microtech) and collected in an antifreeze solution and conserved at −20°C. After inactivation of endogenous peroxidases and blocking with Avidin/Biotin Blocking Kit (Vector Labs, USA), sections were processed with a combination of FITCH coupled riboprobe against mouse CB1 receptor (1:1000, prepared as described in Marsicano and Lutz, 1999) together with Digoxigenin (DIG)-labeled riboprope against D1R or D2R (1:1000 Monory et al., 2007). Signals were revealed with a TSA reaction using fluorescein isothiocyanate (FITC)-labeled tyramide (1:80 for 12 minutes, Perkin Elmer) for CB_1 receptor, or with Streptavidin-Texas Red (1:400, PerkinElmer) for D1R or D2R receptor. Sense control probes were used to establish background signal. After processing for FISH, anti-GFP immunofluorescence was carried out as previously described (Oliveira da Cruz et al., 2020; Terral et al., 2019). Counting of co-expressing cells was performed manually over 20x objective fluorescent microscope as previously described (Bellocchio et al., 2010, Oliveira da Cruz et al., 2020; Terral et al., 2019). Image analyses and counting was performed in at least 6 striatal slice per mouse averaging results from 3-4 mice. This resulted in counting 1300-1600 neurons in average per each condition/analysis.

Quantitative real-time PCR (qRT-PCR).

Samples from WT, DN22-*CB_1*-KI and *CB_1*-KO mice were homogenized in Tri-reagent (Euromedex, France) and RNA was isolated using a standard chloroform/isopropanol protocol(Chomczynski and Sacchi, 1987). RNA was processed and analyzed following an adaptation of published methods. cDNA was synthesized from 1 µg of total RNA using Maxima Reverse Transcriptase (Thermo Scientific, USA) and primed with oligo-dT primers (Thermo Scientific,

USA) and random primers (Thermo Scientific, USA). qRT-PCR was perfomed using a LightCycler® 480 Real-Time PCR System (Roche, Switzerland). qRT-PCR reactions were done in duplicate for each sample, using transcript-specific primers, cDNA (4 ng) and LightCycler 480 SYBR Green I Master (Roche, Switzerland) in a final volume of 10 µl. The PCR data were exported and analyzed in an informatics tool (Gene Expression Analysis Software Environment) developed at the NeuroCentre Magendie. For the determination of the reference gene, the Genorm method was used(Livak and Schmittgen, 2001). Relative expression analysis was corrected for PCR efficiency and normalized against two reference genes. Valosin containing protein (Vcp) and succinate dehydrogenase complex subunit (Sdha) genes were used as reference genes for Amygdala. Glyceraldehyde-3-phosphate dehydrogenase (Gapdh) and Sdha genes were used as reference genes for Hippocampus. Tubulin alpha 4 a (Tuba4a) and tyrosine 3 mono oxygenase tryptophan 5 mono oxygenase activation protein zeta (Ywhaz) genes were used as reference genes for Anterior Olfactory Nucleus. Sdha and tubulin alpha 4 a (Tuba4a) genes were used as reference genes for Prefrontal Cortex. Actin, beta (Actb) and tTubulin alpha 4 a (Tuba4a) genes were used as reference genes for STR. Glyceraldehyde-3-phosphate dehydrogenase (Gapdh) and peptidylprolyl isomerase A (Ppia) genes were used as reference genes for Hypothalamus. The relative level of expression was calculated using the comparative ($2^{-\Delta CT}$) method(Livak and Schmittgen, 2001). Primers sequences are reported in the following table:

Gene	GenBank ID	Forward Sequence (5'-3')	Reverse Sequence (5'-3')
Vcp	NM_009503	TGGCCGTCTAGATCAGCTCAT	TTTCGCAGATTGGCTTTTAGG
Sdha	NM_023281	TACAAAGTGCGGGTCGATGA	TGTTCCCCAAACGGCTTCT
Gapdh	NM_008084	TCAAGAAGGTGGTGAAGCAG	TGGGAGTTGCTGTTGAAGTC
Tuba4a	NM_009447	CCACTTCCCCTTGGCTACCTA	CCACTGACAGCTGCTCATGGT
Ywhaz	NM_011740	CTTGTGAGGCTGTGACACAAAC	CAAGAGTGTGCACGCAGACA
Actb	NM_007393	TGACCGAGCGTGGCTACA	CATAGCACAGCTTCTCTTTGATGTC
Ppia	NM_008907	CAAATGCTGGACCAAACACAA	GCCATCCAGCCATTCAGTCT
Cnr1	NM_007726	GTCGATCTTAGACGGCCTTGC	TTGAGCCCACGTAGAGGAGGT
Cnr1	NM_007726	GTGCTGTTGCTGTTCATTGTG	CTTGCCATCTTCTGAGGTGTG

Mitochondrial respiration

Mitochondrial respiration in substantia nigra extracts was measured as previously described(Hebert-Chatelain et al., 2016) with some modification. Briefly, immediately after cervical dislocation, the mouse brain was extracted and the substantia nigra was rapidly dissected using the coronal brain matrix(Vallee et al., 2014) and was homogenized in 450 μl of Miro5 buffer without taurine supplementation (Makrecka-Kuka et al., 2015) using a Politron homogenizer (11.000 rpm 3-5 sec). After brief centrifugation the supernatant was treated with saponin at a final concentration of 12.5 μg/ml. Respiration analyses were carried out using a 2K Oroboros device(Makrecka-Kuka et al., 2015). 100 µl of lysate were put in each chamber and complex I-dependent

respiration was triggered by adding malate (2mM), pyruvate (5mM) and glutamate (10 mM) (MPG)(Makrecka-Kuka et al., 2015). Then we applied DMSO or WIN 55,212-2 at final concentration of 1μM and 5 minutes after we injected 1.25 mM ADP. Each measure of OCR in ADP condition was normalized to the values before ADP injection and the effect of WIN 55,212-2 was expressed as percentage of vehicle conditions. Only samples for which the ratio of ADP/MPG in the vehicle was equal or superior to 1.5 were retained for the analyses. In the experiments of KH7 pre-treatment, the drug was dissolved in DMSO (used as vehicle) and injected together with the lysates at a final concentration of 5µM.

In a previous set of experiments we validated the quality of mitochondria in the preparation by measuring the O_2 consumption after the MPG and ADP administration. We added the complex II substrate Succinate at the final concentration of 10mM, 10µM Cytochrome C, to check mitochondrial membrane integrity, and finally Rotenone (0.5µM) and Antimycin A (2.5µM) inhibitors of complex I and III, respectively(Makrecka-Kuka et al., 2015) (**Table S1**). When using homogenates from virus-injected mice (see above) 40ul of samples were processed for western blotting against sAC, HA-tag and myc-tag to confirm overexpression of mt-sAC and the different forms of PKA-CA in the SNr of D_1-Cre mice respectively.

Mitochondrial isolation from mouse striatum

In this set of experiments, D_1-Cre mice were injected with control AAV vector, AAV-DIO-mt-sAC-HA, AAV-DIO-PKA-CA and AAV-DIO-MLS-PKA-CA as described above. Mice were sacrificed by cervical dislocation, brains were

rapidly extracted and the striatum dissected on ice. Mitochondria were extracted by immuno-magnetic isolation using the Mitochondrial Extraction and Isolation Kits (Milteny Biotech, FRANCE) according to manufacturer instructions. After tissue lysis in 1.5ml of protease inhibition buffer provided by the manufacturer, one small fraction was collected as total cell lysate (TCL). Extracted mitochondria and their respective TCL were re-suspended in the same buffer, quantified for their protein content and loaded on polyacrylamide gel (12µg per sample) for western blotting as described below.

Western Blotting

Protein homogenates in Miro5, added with protease inhibitors (Complete protease inhibitor cocktail, Sigma-Aldrich, France) have been mixed with denaturing 4x Laemmli loading buffer (250 mM Tris-HCl, 40% Glycerol, 8% SDS, 5% β-Mercaptoethanol, 0.2% Bromophenol blue) and boiled at 95°C for 5 minutes. Samples were analyzed on 4-20% precast polyacrylamide gels (Bio-Rad, Hercules, California) and transferred onto PVDF membranes 0.45µm (Merk Millipore, Burlington, MA). Membranes were blocked in a mixture of Tris-buffered saline and polysorbate 20 (20mM Tris-HCl pH 7.6, 150mM NaCl, 0.05% Tween 20) containing 5% of non-fat dry milk for 1 h at room temperature. For immunoblotting have been used antibodies against HA-Tag (#3724; 1:1000, Cell Signaling Technology Danvers, MA or #PA1-985; 1:1000, Thermo Fisher Scientific, Waltham, MA), myc-tag (#11667149001; 1:500, Merk, Darmstadt, Germany), sAC (ADCY10 PA-543049; 1:1000, Thermo Fisher Scientific, Waltham, MA), TOMM20 (#sc-111415, 1:1000, Santa Cruz Biotechnology, Dallas, Texas), PKA catalytic subunit (#Ab76238, 1:2000, Abcam, Cambridge,

UK) and Tubulin (sc-69969; 1:5000, Santa Cruz Biotechnology, Dallas, Texas) . Bound primary antibodies were detected with HRP-linked antibodies (1:2000, Cell Signaling Technology, Danvers, MA) and visualized by enhanced chemiluminescence detection (Clarity Western ECL Substrate, Bio-Rad, Hercules, California or Super Signal West Femto Maximum Sensitivity Substrate, Thermo Fisher Scientific, Waltham, MA) The images have been acquired on ChemiDoc Touch (Bio-Rad, Hercules, California and analysed using the Image Lab software (Bio-Rad, Hercules, California)

[^{35}S]GTPγS binding assay on brain homogenates

Brains from 8 mice of each genotype (WT, *CB_1*-KO and DN22-*CB_1*-KI) were obtained. Midbrain, cortex and hippocampus were dissected and immediately stored at −70 °C until assay. For each brain region, tissue samples from each genotype were pooled to obtain the enriched fractions of plasma membranes. Tissue samples were homogenized using an a Teflon-glass grinder (IKA Labortechnik, Satufen, Germany) at 1500 rpm (10 up-and-down strokes) in 30 volumes of homogenization buffer (1 mM EGTA, 3 mM $MgCl_2$, 1 mM DTT, and 50 mM Tris-HCl, pH 7.4) supplemented with 0.25 M sucrose. The crude homogenate was centrifuged for 5 minutes at 1,000 x g at 4 ºC and the supernatant layer was re-centrifuged for 10 minutes at 40,000 x g (4ºC). The resultant pellet (P2 fraction) was washed twice in 10 and 5 volumes of homogenization buffer respectively, and re-centrifuged in similar conditions. Protein content was measured according to Bradford's method using BSA as standard. Samples were aliquoted in order to have a protein content of 1 mg and then centrifuged in a benchtop centrifuge (EBA 12 R, Hettich Instruments,

Tuttlingen, Germany) at highest speed (14,000 rpm) during 15 minutes at 4 ºC. The supernatant layer was carefully discarded and the pellets stored at -70 ºC until assay. The tissue samples of the nine experimental conditions (3 genotypes and 3 brain regions, 1 pool for each region-genotype) were processed in parallel on the same day. The day of the experiment the membrane pellets were defrosted (4ºC), thawed and re-suspended in 11 ml of incubation buffer containing 1 mM EGTA, 3 mM $MgCl_2$, 100 mM NaCl, and 50 mM Tris-HCl, pH 7.4, reaching a final protein concentration of 0.09 mg/ml approximately. The real final protein content was measured after the experiment according to Bradford's method.

WIN 55,212-2 stimulated [^{35}S]GTPγS binding assays were carried out in a final volume of 250 µl in 96 well plates, containing 1 mM EGTA, 3 mM $MgCl_2$, 100 mM NaCl, 0.2 mM DTT, 50 µM GDP, 50 mM Tris–HCl at pH 7.4 and 0.5 nM [^{35}S]GTPγS. Stimulation curves were carried out by incubating increasing concentrations of WIN 55,212-2 (10^{-12}-10^{-4} M; 9 concentrations by duplicate; three independent experiments). The incubation was started by addition of the membrane suspension (18 µg of membrane proteins per well) and was performed at 30ºC for 120 minutes with shaking (450 rpm). Incubation was terminated by rapid filtration under vacuum (1450 FilterMate Harvester, PerkinElmer) through GF/C glass fiber filters (Printed Filtermat A) pre-soaked in ice-cold incubation buffer. The filters were then rinsed three times with 300 µl ice-cold incubation buffer, air dried (20°C, 120 minutes), and counted for radioactivity (4 minutes) by liquid scintillation spectrometry using a MicroBeta TriLux counter (PerkinElmer). Non-specific binding of the radioligand was

defined as the remaining [^{35}S]GTPγS binding in the presence of 10 μM unlabelled GTPγS, and the basal binding, as the signal in the absence of agonist. The pharmacological parameters of the stimulation curves of the [^{35}S]GTPγS binding, the maximal effect (Emax) and the concentration of the drug that determines the half maximal effect (EC50), were obtained by non-linear analysis using GraphPad Prism™ software version 5.0. The points fit to a concentration-response curve (standard slope). The pharmacological parameters Emax and EC50 are expressed as means ± SEM. The statistical comparison of the data sets was performed in GraphPad Prism™ software version 5.0, by a co-analysis of the curves.

[^{35}S]GTPγS and [^{3}H]CP55,940 binding assay on brain slices

[^{35}S]GTPγS (1250 Ci/mmol) and [^{3}H]CP55,940 (149 Ci/mmol) were purchased from PerkinElmer (Boston MA, USA). The [^{14}C] and [^{3}H] standards were supplied by American Radiolabelled Chemicals (St. Louis, MO, USA). DL-dithiothreitol (DTT), guanosine-5'-diphosphate (GDP), and guanosine-5'-γ-3-thiotriphosphate (GTPγS) were acquired from Sigma-Aldrich (St. Louis, MO, USA). WIN 55,212-2 was purchased from Tocris Bioscience (Bristol, UK). All other chemicals were obtained from standard sources and were of the highest purity commercially available.

In order to test the ability of CB_1 receptor to stimulate GTPγS conversion after WIN 55,212-2 administration or to bind the CP55,940 agonist, 5-6 WT and DN22-*CB_1*-KI mice, and 1 *CB_1*-KO mouse as control, were sacrificed by cervical dislocation and their brain rapidly frozen at -80°C. 20μm slices were cut with a cryostat and mounted on superflost (Thermo Scientific, FRANCE) slides.

[^{35}S]GTPγS binding assay. Brain sections were thawed for 15 min and then incubated in 50 mM Tris-HCl buffer with 3 mM $MgCl_2$, 0.2 mM EGTA, 100 mM NaCl, 2 mM GDP and 1 mM DTT (pH = 7.4) for 20 min at room temperature. Afterwards, the slices were incubated with 0.04 nM [^{35}S]GTPγS in absence and in presence of WIN 55,212-2 μM (1 and 10 μM) for 2 h at 30ºC. The non-specific binding was determined with 10 μM GTPγS. Finally, the sections were washed twice in 50 mM Tris-HCl (pH =7.4) for 15 min at 4ºC, dried and exposed to a Kodak Biomax MR film with ^{14}C standards. The films were scanned and quantified by transforming the optical densities into nCi/mg using the ^{14}C standards (NIH-IMAGE, Bethesda, MA, USA). The background and the non-specific densities were subtracted. The percentages of stimulation were calculated from the basal and agonist-stimulated [^{35}S]GTPγS binding densities according to the formula (stimulated x 100/basal) - 100.

[^{3}H]CP55,940 binding assay. Tissue sections were dried and incubated in 50 mM Tris-HCl buffer containing 1% of BSA (pH = 7.4) for 30 min at room temperature. Later, the brain sections were incubated again in the same buffer supplemented with 3 nM [^{3}H]CP55,940 for 2h at 37ºC. Non-specific binding was determined with 10 μM WIN 55,212-2. Finally, sections were washed in ice-cold 50 mM Tris-HCl buffer supplemented with 1% BSA followed by dipping in distilled water at 4ºC. After drying, the brain slides were exposed to a radiation sensitive film for 21 days at 4ºC together with tritium standards. The films were scanned and quantified by transforming the optical densities into nCi/mg using the tritium standards (NIH-IMAGE, Bethesda, MA, USA). The background and the non-specific densities were subtracted to determine the specific binding.

Behavioral tests

Wire hang test. Wild type and DN22-*CB_1*-KI mice were tested for their muscular strength in the wire hang test(Redon et al., 2020). All tests were conducted during the dark phase of the cycle under dim red light. Each cage, housing one mouse, was placed on a bench in a room adjacent to the one housing the mice. Thereafter, each mouse was removed from its cage, placed on the cage grid, the latter being then slowly inverted as to be suspended 90 cm above a big cage filled with polystyrene beads. The latency to fall was then recorded.

Basal locomotion. The basal locomotor activity of WT and DN22-*CB_1*-KI mice was measure during seven days using the TSE PhenoMaster system (TSE Systems GmbH). Mice were placed individually in a plexiglass cage [45cm (length) X 34cm (width) X 20cm (height)] surrounded with the ActiMot module containing IR light beams recognizing locomotor activity. Food and water were available *ad libitum.*

Catalepsy, locomotion and antinociception. AM251 and Hemopressin were bilaterally injected into the SNr in a volume of 0.5 µl per side. Immediately after, THC (10 mg/kg) was injected i.p. Mice were tested, 30 min post-injections, successively for catalepsy, locomotion and antinociception. Locomotor activity was tested by placing the mouse in a novel environment and the number of squares crossed was counted for 5 minutes. For seek of clarity, given the fact that striatonigral CB_1 receptor deletion did not affect the hypo-locomotor effects of THC (**Figure S1B and S1E**), we did not show results for this behavioral paradigm for the other experimental sets. The catalepsy was determined by the time of immobility on a bar. To this aim, mice were positioned in a new plastic

cage (identical to their home cage) without bedding with on a horizontal cylindrical bar (0.7cm Diameter) placed at 4.5 cm high with their forepaws gripping and its hind paws in the plastic box. The time spent in its initial position on the bar was scored for two minutes. Immediately after, mice were placed in a Hot Plate (BIOSEB) to measure antinociception. The plate was pre-heated at 52°. The escape latency, defined as the time until the mice showed signs of discomfort (paw licking, jumping), was recorded. All equipment was cleaned with ethanol 25% and dried with paper towels between all the trials. For AAVs injected mice the procedure was identical but mice were tested 5 weeks after viral injections.

Immuno-electron microscopy

The experiments were performed as described previously(Puente, 2019). CB_1-KO, DN22-CB_1-KI, and respective WT littermates mice (n = 3 per genotype) were deeply anesthetized by intraperitoneal injection of ketamine/xylazine (80/10 mg/kg body weight i.p.) and were transcardially perfused at room temperature (RT, 20-25°C) with phosphate buffered saline (0.1 M PBS, pH 7.4) for 20 s, followed by the fixative solution made up of 4% formaldehyde (freshly depolymerized from paraformaldehyde), 0.2% picric acid, and 0.1% glutaraldehyde in phosphate buffer (0.1 M PB, pH 7.4) for 10-15 min. Once the animals were perfused, the brains were numbered by a different experimenter to conduct the protocol blindly. Then, brains were removed from the skull and post-fixed in the fixative solution for approximately 1 week at 4°C. Afterwards, brains were stored at 4°C in 1:10 diluted fixative solution until used.

Pre-embedding silver-intensified immunogold method. The method applied was already described(Puente, 2019). Coronal midbrain vibratome sections containing the substantia nigra pars reticulata were cut at 50 μm and collected in 0.1 M PB (pH 7.4) with 0.1% sodium azide at RT. Sections were preincubated in a blocking solution of 10% bovine serum albumin (BSA), 0.1% sodium azide, and 0.02% saponin prepared in Tris-HCl buffered saline (TBS 1X, pH 7.4) for 30 min at RT. Then, sections were incubated with a primary goat anti-CB_1 antibody binding to a 31 amino acids sequence of the C-terminus (CB_1 C-ter[31]; 2 µg/ml; Cat. N.: CB_1-Go-Af450-1; Frontier Institute; Japan) in the blocking solution but with 0.004% saponin on a shaker for 1 day at RT. After several washes in 1% BSA/TBS, tissue sections were incubated in a secondary anti-goat 1.4 nm gold-labeled Immunoglobulin-G antibody (Fab' fragment, 1:100, Nanoprobes Inc.) in 1% BSA/TBS with 0.004% saponin on a shaker for 4 h at RT. Thereafter, the tissue was washed in 1% BSA/TBS overnight at 4°C and post-fixed in 1% glutaraldehyde in TBS for 10 min at RT. Following washes in double distilled water, gold particles were silver-intensified with a HQ Silver kit (Nanoprobes Inc., Yaphank, NY, USA) for about 12 min in the dark and then washed in 0.1 M PB (pH 7.4). Stained sections were osmicated (1% osmium tetroxide, OsO_4, in 0.1 M PB pH 7.4, 20 min), dehydrated in graded alcohols to propylene oxide, and plastic-embedded flat in Epon 812. To localize the region of interest, immunolabeled resin-embedded vibratome sections were first visualized by light microscopy to select the portion of the SN and to ensure that the slices have the appropriate antibody labeling. Then, semithin (700 nm) sections are mainly extracted to remove the resin and reach the tissue. Afterwards, we started to collect ultrathin sections of 50 nm on mesh nickel

grids, stained with 2.5% lead citrate for 20 min, and examined in a Philips EM208S electron microscope. Photographs are always taken in the area of interest and close to the resin; in this way we know that we are a few nanometers from the surface, and that the immunelabeling is complete. Furthermore, we photographed in a range of 0 to at most 950 nm from the surface, because the first 5 ultrathin sections of 50 nm are collected. Tissue preparations were photographed by using a digital camera coupled to the electron microscope. Figure compositions were made at 300 dots per inch (dpi). Labeling and minor adjustments in contrast and brightness were made using Adobe Photoshop (CS, Adobe Systems, San Jose, CA, USA).

Semi-quantification of mtCB$_1$ receptor immunostaining using immunogold method. Analyses were carried out according to previous publications (Gutierrez-Rodriguez et al., 2018; Hebert-Chatelain et al., 2016; Puente et al., 2019). 2-3 of 50 µm-thick sections containing the substantia nigra pars reticulata and hippocampus from each animal genotype (n=3 each) showing good and reproducible silver-intensified gold particles were cut at 50 nm. To minimize differences between groups, all sections were processed simultaneously. Three separate experiments were performed for each animal. Electron micrographs were taken from grids with similar labeling intensity indicating that selected areas were at the same depth. To avoid false negatives, only ultrathin sections in the first 1.5 µm from the surface were examined. Total CB$_1$ receptor labeling and total CB$_1$ particles in plasma and mitochondrial membranes were counted per area. The proportion of CB$_1$ receptor-positive mitochondria was calculated for each mouse counting only particles (at least one) on mitochondrial membrane segments far away from other membranes

(distance ≥ 80 nm). Image-J (version 1.36) was used to measure the distance. Graphs and statistical analyses were performed using GraphPad software (version 5.0).

***In vitro* characterization of mt-sAC and PKA mutants**

Confocal Microscopy Imaging. HeLa cells seeded on 12-mm round glass coverslips and transfected as indicated, were placed on the stage of the Olympus FV3000 confocal fluorescence microscope (Tokyo, Japan) and imaged using a 60X oil objective (UPLAN 60× oil, 1.35 NA, Olympus), and appropriate excitation laser and filters. For each experiment, 15 cells were randomly selected and analyzed. Stacks of 30 images separated by 0.2 µm along the Z axis were acquired. Three-dimensional reconstruction and volume rendering of the stacks were carried out with the appropriate plug-in of ImageJ (NIH, Bethesda, MD, USA). Pearson's correlation coefficient for TOM20 fluorescence colocalization with Myc or HA, was calculated with the Colocalization threshold tool of ImageJ.

Trypsin Sensitivity Assay. The trypsin sensitivity assay was carried out as described previously (Choo, 2004) with minor modifications. Isolation of mitochondrial fractions was performed as described previously (Guedouari et al., 2017). Briefly, HeLa cells were harvested and resuspended in mitochondrial isolation buffer (250 mM sucrose, 1 mM EDTA, 5 mM HEPES, pH 7.4) supplemented with 1% protease inhibitor cocktail (Bioshop, ON, Canada), 2 mM sodium orthovanadate and 1 mM sodium fluoride. Cells were lysed with 15 strokes using a 25-gauge syringe on ice and centrifuged at 1500× g for 5 min (4 °C). The resulting supernatant was centrifuged at 12,500× g for 10 min (4 °C). pellet was resuspended in the mitochondrial buffer and a cycle of centrifugation

at 1500× g and 12,500× g was repeated. The final pellet was considered as the mitochondria-enriched fraction. Protein concentration was determined by Bradford assay (Bradford, 1976). Isolated mitochondria were suspended in mitochondrial isolation buffer and incubated at 37 °C for 10 min in presence or absence of trypsin (0.5%) and triton X-100 (1%). Reaction was stopped by the addition of 1% of the protease inhibitor cocktail. Mitochondria were then centrifuged at 12,500× g at 4 °C for 10 min. The pellets were processed for SDS-PAGE and subsequent western blotting.

Sniffer cells detection of Substance-P release

cDNA for human NK_1 was purchased from the cDNA resource center (www.cdna.org). NK_1-mCherry plasmid was created by cloning the mCherry coding sequence in frame with the C-terminus of NK_1 with its stop codon removed by PCR.

System validation in vitro. NK_1-mCherry was co-transfected with GCaMP6s (Addgene) into HEK293 cells (Cedarlane) seeded on coverslips using Lipofectamine 2000 (Invitrogen). 24-48 hours later, coverslips were transferred to a perfusion chamber containing EBS (in mM: NaCl 140, KCl 5.4, $CaCl_2$ 1.3, HEPES 10, glucose 33, pH 7.35) and allowed to equilibrate for 10-15 minutes at room temperature with a flow rate of ~1ml/min. Baseline GCaMP6s fluorescence was recorded for 60 seconds. Then Substance-P (Tocris) was added to the chamber using a micropipette to achieve final concentrations of 10^{-11}M-10^{-6}M. 16-bit Images were collected at 1Hz on an Olympus BX-61 microscope with a 20X water immersion objective and a Hamamatsu ORCA-Flash4 CCD camera. Using ImageJ, the change in fluorescence normalized to baseline fluorescence ($\Delta F/F0$) was calculated following background subtraction

by binning the 30 frames prior to Substance-P stimulation (F0) and 30 frames surrounding the peak response following Substance-P stimulation. The perfusion chamber was washed with 50mL of EBS over 15 minutes between coverslips. When necessary, rundown was corrected using the Bleach Correction algorithm in ImageJ and the occasional flicker of the microscope bulb was corrected manually.

Substance-P and WIN 55,212-2 *effect in vitro.* HEK cells were seeded on glass coverslips coated with poly-lysine and transfected with plasmid DNA for NK_1-mCherry and GCaMP6s or Empty vector and GCaMP6s with PEI (**Figure S1I**). Cells were imaged 24-48 hrs after transfection on epifluorescence mode with an inverted spinning-disk microscope equipped with 40X objective (NA 1.4), a multi-LED illumination system and a CDD camera. Coverslips were mounted on a open chamber and superfused with a buffer solution of (in mM): 112 NaCl, 5 KCl, 24 NaHCO3, 10 HEPES, 1.25 $CaCl_2$, 1.25 $MgCl_2$, 5 glucose, bubbled with air/5% CO_2 (pH 7.4) at 36°C. For experiments on cells expressing NK_1-mCherry/ GCaMP6s, cells expressing NK_1 were first selected by 570 nm illumination and emission collection at 617/36 nm before starting Ca^{2+} imaging. Cells expressing GCaMP6s were excited at 490 nm for 0.05-0.1 s and emission collected at 524/16 nm. Data was background corrected and represented as normalized fluorescence. Substance-P and WIN55.212-2 were applied for 1 minute and recording were performed for the next 5 minutes (**Figure S1L**).

Substance-P release from striatonigral terminals. Sagittal sections containing SNr were prepared from 6 to 12 weeks-old mice. For electrical stimulation, naive CB_1-KO, DN22-CB_1-KI, and respective WT littermates were used. For optogenetic activation of striatonigral terminals 6 weeks-old D1-Cre mice were

used to target striatal neurons with injection of a rAAV-hSyn-DIO-ChrimsonR-tdTomato into the dorsal Striatum (in mm relative to bregma: AP=+0.8, L=±2.0, DV=-2.7) 6 weeks before experiments.

Mice were first sedated by inhaling isoflurane (4%) for approximately 30 s and then deeply anesthetized with a mixture of ketamine and xylazine (100 and 20 mg/kg, i.p., respectively). After the disappearance of the reflexes, a thoracotomy was performed to allow transcardial perfusion of a saturated (95% O_2/5% CO_2) ice-cold solution containing 250 mM sucrose, 10 mM $MgSO_4 \cdot 7H_2O$, 2.5 mM KCl, 1.25 mM $NaH_2PO_4 \cdot H_2O$, 0.5 mM $CaCl_2 \cdot H_2O$, 1.3 mM $MgCl_2$, 26 mM $NaHCO_3$ and 10 mM D-glucose. After decapitation, each brain was quickly removed and cut into sagittal slices (300 µm) using a vibratome (VT-1200S; Leica Microsystems, Germany). The slices were then incubated at 34°C for 10 min in a standard artificial cerebrospinal fluid (ACSF) saturated by bubbling 95% O_2/5% CO_2 and containing 126 mM NaCl, 2.5 mM KCl, 1.25 mM $NaH_2PO_4 \cdot H_2O$, 2 mM $CaCl_2 \cdot H_2O$, 2 mM $MgSO_4 \cdot 7H_2O$, 26 mM $NaHCO_3$ and 10 mM D-glucose, supplemented with 5 µM glutathion and 1 mM sodium pyruvate.

Transfected HEK cells (*see above*) re-suspended in ACSF were gently deposited over the slices that were placed in a small petri-dish. Slices were allowed to rest for 2h to allow the sniffer cells to attach to the tissue before starting the recording. Slices were then transferred in a recording chamber under an upright microscope (Ni-E, Nikon Instruments). For electrical stimulation experiments, a bipolar stimulating electrode was placed in proximity of *capsula interna* and trains of electrical stimulation were applied. For optogentic activation, an optic fiber was placed above the SNr and trains of 570nM light pulses (5s 20 Hz) were applied. The presence of the receptor and

the fluorescence of GCaMP6s in HEK cells were observed and measured with an infrared differential interference system using a 60x immersion lens. The image detection was done with a camera (Zyla, Andor technology). GCaMP6s was excited using 470 nm light supplied by a LED device (Lumencor). Images were collected at 10 Hz. Image stacks were imported into Image J software where changes in fluorescence in HEK cell were measured over time. Imaged were post-processed to calculate ΔF. Regions of interest (ROI) corresponded to HEK cell visually identifiable and expressing both GCaMP6s and Substance-P Receptor were delimited. The fluorescence time course F of each ROI was measuring by averaging all pixels within the ROI. Background fluorescence was subtracted from all values. Fluorescence at various time points was expressed relative to baseline. Stimulus-induced changes in fluorescence were calculated from the maximum value observed during a 30 s period following the onset of the response and expressed relative to baseline (average of values collected 10 s before the electrical stimulation or 3 s before red-light stimulation). Negative controls on brain slices were performed either by using HEK cells transfected only with GCaMP6s and not NK1-R (*see above*) or by GCaMP6s/NK1-R expressing HEK cells in presence of the selective Substance-P Receptor blocker CP122721. Control experiments for whole-cell voltage-clamp recordings of oIPSCs were performed as described in the next session.

Electrophysiology

Optogenetic activation of striatonigral terminals. Male DN22-CB_1-KI mice, CB_1-KO mice and their WT littermates were used to target striatal neurons with injection of a AAV2-hSyn-ChR2(H134R)-mCherry into the dorsal Striatum (in

mm relative to bregma: AP=+0.8, L=±2.0, DV=-2.7) 8-9 weeks before electrophysiological recordings. Mice were sedated with isoflurane, deeply anesthetized with ketamine/xylazine (75/10 mg/Kg) and perfused transcardially with ice-cold modified artificial cerebrospinal fluid (ACSF), equilibrated with 95% O_2 and 5% CO_2, and containing (in mM): 230 sucrose, 26 $NaHCO_3$, 2.5 KCl, 1.25 NaH_2PO_4, 0.5 $CaCl_2$, 10 $MgSO_4$ and 10 glucose. Brains were rapidly removed and sectioned into 300 µm-thick parasagittal slices with a vibrating blade microtome (VT1200S; Leica Microsystems, Germany). Slices containing the SNr were then left to equilibrate for 1 h (at 35°C) in ACSF of the following composition (in mM except otherwise specified): 126 NaCl, 26 $NaHCO_3$, 2.5 KCl, 1.25 NaH_2PO_4, 2 $CaCl_2$, 2 $MgSO_4$, 10 glucose, 1 sodium pyruvate and 4.9µM L-gluthathione reduced (gassed with 95% O_2 and 5% CO_2). Single slices were transferred to a recording chamber, perfused continuously with modified oxygenated ACSF at 32-34°C containing (in mM): 126 NaCl, 26 $NaHCO_3$, 3 KCl, 1.25 NaH_2PO_4, 1.6 $CaCl_2$, 1.5 $MgSO_4$, 10 glucose, and visualized using infrared gradient contrast video microscopy and a 60X water-immersion objective (Fluor 60X/1.00 W, Nikon). Recordings from individual SNr neurons were made using pipettes (impedance, 6-8 MΩ) prepared from borosilicate glass capillaries (G150-4; Warner Instruments, Hamden, CT, USA) with a micropipette puller (P-97; Sutter Instruments, Novato, CA, USA). For whole-cell voltage-clamp recordings, pipettes were filled with (in mM): 130 K-gluconate, 6.6 Na-gluconate, 1 $MgCl_2.6H_2O$, 10 HEPES, 5 QX-314, 0.1 Na_4EGTA, 0.4 Na_3GTP, 2 $Mg_{1.5}ATP$ and 5.4 biocytin. The pipette solution had a pH of 7.2 and an osmolarity of 292 mOsm. Recordings were obtained using a Multiclamp 700B amplifier and Digidata 1440 digitizer controlled by Clampex 10.3

(Molecular Devices, Sunnyvale, CA, USA). Signals were low-pass filtered at 4 kHz and sampled at 20 kHz. Whole-cell voltage clamp recordings with Kgluconate-filled electrodes were corrected for a junction potential of 13 mV. In voltage clamp experiments, series resistance was monitored by a step of -5 mV at the end of each recording. Optogenetic activation of SNr terminals was performed *via* optic fiber as previously described (Froux et al., 2018)

After 5 minutes baseline, CB_1 receptor was activated with 5 µM WIN 55,212-2 dissolved in DMSO. This concentration has been previously showed to reduce hippocampal EPSCs in a CB_1 dependent manner(Hebert-Chatelain et al., 2016). The glutamatergic synaptic transmission was not blocked for all electrophysiological experiments. Levels of drug-induced depression in response to WIN 55,212-2 are reported as averaged IPSC amplitudes for 5 min just before bath application compared with averaged IPSC amplitudes during the 15-min period after the application. Data were discarded when the series resistance varied by >20%. After electrophysiological recordings, slices were fixed overnight in a solution of paraformaldehyde at 4% and maintained in PBS-azide at 0.3% at 4°C until histological processing for mCherry visualization or TH/biocytin immunostaining(Chazalon et al., 2018).

Hippocampal depolarization-induced suppression of inhibition. Male DN22-*CB_1*-KI mice and their WT littermates were sacrificed by dislocation and the brain was immediately immerged in ice-cold oxygenated cutting solution containing in mM: 180 Sucrose, 26 $NaHCO_3$, 12 $MgSO_4$, 11 Glucose, 2.5 KCl, 1.25 NaH_2PO_4, and 0.2 $CaCl_2$, oxygenated with 95% O_2-5% CO_2 ≈300mOsm. Parasagittal hippocampal slices (300µm thick) were obtained using a vibratome (VT1200S, Leica, Germany) and transferred for 30min into a 34°C bath of

oxygenated ACSF containing in mM: 123 NaCl, 26 $NaHCO_3$, 11 Glucose, 2.5 KCl, 2.5 $CaCl_2$, 1.3 $MgCl_2$, 1.25 NaH_2PO_4 ≈305 mOsm. After a minimum of 1h recovery at room temperature (22-25°C), slices were transferred to a recording chamber in ACSF at 32°C. Whole-cell recordings of IPSCs were made using a MultiClamp 700B amplifier (Molecular devices, UK) in CA1 pyramidal neurons voltage clamped at −70mV with a pipette (3-5 MΩ) containing in mM: 130 KCl, 10 HEPES, 1 EGTA, 2 $MgCl_2$, 0.3 $CaCl_2$, 7 Phosphocreatin, 3 Mg-ATP, 0.3 Na-GTP; pH = 7.2; 290mOsm. Evoked IPSCs were performed by a monopolar stimulating patch pipette filled with ACSF in stratum radiatum in presence of NMDA and AMPA/Kainate receptor antagonists (50µM D-APV and 10µM NBQX).

DSIs were performed by depolarizing pyramidal neurons from −70mV to 0mV for 3 s. DSIs' magnitude were measured as the average of 3 DSIs with 2min apart and represented the percentage of change between the mean of the 5 consecutive IPSCs preceding the depolarization and the first three IPSCs following the depolarization, with IPSCs evoked every 3 s. Currents were filtered at 4kHz by a Digidata 1440A (Molecular devices, UK) and were analyzed using either Clampfit software (pClamp10).

Data collection and statistical analyses

No statistical methods were used to pre-determine sample sizes, but they are similar to those reported in previous publications. Data collection and analysis were performed blind to the conditions of the experiment. All mice were assigned randomly to the different experimental conditions.

All graphs and statistical analyses were performed using GraphPad software (version 5.0, 6.0 or 8.0). Results were expressed as means of independent data points ± s.e.m. Behavioral data where checked for normality distribution with the D'Agostino&Pearson test. When all groups of an experiment passed the normality test, ANOVA (One-way or Two-way, where appropriate) analysis was performed and when interaction was significant Tukey's post hoc analysis was used. When the normality was rejected, non-parametric One-way ANOVA (Kruskal-Wallis) was used (**Table S2 and S3**). Biochemical, anatomical, imaging and electrophysiological data were analyzed using Student's *t*-test (unpaired or paired, where appropriate) or Wilcoxon test as appropriate (**Table S2 and S3**). Post hoc significances were expressed as follow: * $p<0.05$, ** $p<0.01$, *** $p<0.001$.

FIGURE LEGENDS

Figure 1. Striatonigral CB_1 receptors mediate catalepsy and antinociception.

(**A and B**) Effects of correct "hit" or misplaced "no-hit" intra-SNr administration of the cell permeable CB_1 antagonist AM251 on the (**A**) cataleptic, and (**B**) antinociceptive THC effect (10mg/kg i.p.) respect to vehicle treated mice.

(C) Representative micrograph (left) and relative quantification (right) of CB_1 immunoreactivity in the GPe (white bars) and the SNr (black bars) of mice with striatopallidal (ST-GP-*CB_1*-KO) or striatonigral (ST-SN-*CB_1*-KO) CB_1 receptor deletion compared to control littermates. Target regions are indicated by yellow dotted lines.

(D) Cataleptic and **(E)** antinociceptive effects of THC (10mg/kg i.p.) in mice with striatopallidal (ST-GP-*CB_1*-KO) or striatonigral (ST-SN-*CB_1*-KO) CB_1 receptor deletion compared to control littermates.

(**F and G**) Effects of intra-SNr administration of the cell impermeable CB_1 antagonist Hemopressin (Hp) on the **(F)** cataleptic, and **(G)** antinociceptive effect of systemic THC (10mg/kg i.p.) respect to vehicle treated mice.

(H and I) Effects of intra-SNr administration of the NK_1 receptor agonist GR73632 on the (**H)** cataleptic, and **(I)** antinociceptive effect of THC (10mg/kg i.p.) respect to vehicle treated mice.

(J) Schematic representation of the Substance-P sniffer strategy, and representative picture of sniffers cells [HEK cell expressing NK_1 receptor

(NK_1R) (red) and GCaMP6 (green)] deposited over slices (IR). Stim: electrical stimulation, STR: striatum, SNr: Substantia nigra pars reticulata, GPe: external globus pallidus. Scale bars: 50 μm.

(**K)** Left: Representative GCaMP6 fluorescence in the SNr before and after electrical stimulation, in presence of vehicle or WIN (5μM). Middle: traces of GCaMP6 fluorescence variation (ΔF/F0) from sniffer cells overlying the area shown in **(K)** (right panel, white square) in the absence (Vehicle) and in the presence of WIN when electrical stimulation (gray bars) of the striatonigral pathway is applied in both WT and *CB_1*-KO littermates. Plots are from the same cells in both conditions. Right: summary graphs comparing ΔF induced by electrical stimulation in all sniffer cells responding and imaged over the SNr in Vehicle and WIN conditions, comparing WT vs *CB_1*-KO littermates.

(L) Schematic representation of the Substance-P sniffer strategy coupled to optogenetic stimulation of striatonigral terminals. SNr: Substantia nigra pars reticulata, GPe: external globus pallidus.

(M) Left: traces of GCaMP6 fluorescence variation (ΔF/F0) from sniffer cells overlying the SNr in the absence (Vehicle) and in the presence of WIN when light stimulation (red bars) of the striatonigral pathway is applied. Plots are from the same cells in both conditions. Right: summary graphs comparing ΔF induced by light stimulation in all sniffer cells responding and imaged over the SNr in Vehicle and WIN conditions.

Figure 2. CB_1 receptor subcellular localization in the SNr.

(A - E) Immunogold detection of CB_1 receptor by electron microscopy in WT and *CB_1*-KO mice in SNr. White arrows, plasma membrane gold particles; pink arrows, mitochondrial gold particles; scale bar: 500 nm. Den, dendrites; ter, synaptic terminal, m, mitochondrion; red arrowheads, synapses. Relative quantifications of total CB_1 receptor labeling (**B**), plasma membrane CB_1 ($pmCB_1$) receptor labeling **(C)**, mitochondrial-associated CB_1 ($mtCB_1$) receptor labeling **(D)** and proportion of CB_1 receptor-positive mitochondria **(E)**.

(F - J) Immunogold detection of CB_1 receptor by electron microscopy in WT and DN22-*CB_1*-KI mice in SNr. White arrows, plasma membrane gold particles; pink arrows, mitochondrial gold particles; scale bar: 500 nm. Den, dendrites; ter, synaptic terminal, m, mitochondrion; red arrowheads, synapses. Relative quantifications of total CB_1 receptor labeling (**G**), plasma membrane CB_1 ($pmCB_1$) receptor labeling **(H)**, mitochondrial-associated CB_1 ($mtCB_1$) receptor labeling **(I)** and proportion of CB_1 receptor-positive mitochondria **(J)**.

(K) Concentration–response curves of the effect of WIN on [^{35}S]GTPγS binding in membranes isolated from cortex, hippocampus and midbrain of WT, *CB_1*-KO and DN22-*CB_1*-KI mice.

(L) The effect of WIN (1µM) on mitochondrial respiration (oxygen consumption rate, OCR) in SNr homogenates from WT, *CB_1*-KO, and DN22-*CB_1*-KI mice. Data are expressed as percentage of vehicle values.

Figure 3. Striatonigral mtCB$_1$ receptor functions.

(A) Representative picture of the striatonigral pathway targeted with optogenetic tools. STR, striatum; GPe, external globus pallidus; STN, subthalamic nucleus; TH, thalamus; HP, hippocampus; SNr substantia nigra pars reticulata. Scale bar 500µM.

(B) Representative post-hoc characterization of the analyzed cells (white arrow) by immunofluorescence for biocytin, mCherry (ChR2) and thyroxine-hydroxylase (TH). Scale bar: 50µM.

(**C**) Representative traces of light evoked inhibitory post-synaptic currents (oIPSCs) under control condition and in presence of the GABA$_A$ receptor blocker Gabazine (GBZ) with its corresponding time-course effect.

(D) Time course effect of WIN (5 µM) on striatonigral oIPSCs in slices derived from WT, *CB$_1$*-KO and DN22-*CB$_1$*-KI mice.

(**E)** Plots of normalized oIPSCs with representative traces before and after WIN treatment and summary of the average change of oIPSCs relative to baseline.

(**F)** Cataleptic, and **(G)** antinociceptive effect of systemic THC (10mg/kg i.p.) or WIN (3mg/kg i.p.), respect to vehicle in WT and DN22-*CB$_1$*-KI mice

Figure 4. Striatonigral mtCB_1 receptor signaling.

(A) Schematic representation of the CB_1 or DN22-CB_1 rescue-approach in D_1-*CB_1*-KO mice. STR, striatum; SNr, substantia nigra pars reticulata; mtCB_1, mitochondrial CB_1 receptor; pmCB_1, plasma membrane CB_1 receptor.

(B) Representative immunofluorescence pictures of CB_1 or DN22-CB_1 rescue in the SNr of D_1-*CB_1*-KO mice. Green, CB_1 positive signal; Blue, DAPI nuclear counterstaining. Scale bar 250µm.

(C) Relative quantification of CB_1 receptor immunofluorescence D_1-*CB_1*-KO mice after CB_1 or DN22-CB_1 rescue in the SNr.

(D) Effect of WIN (1µM) on mitochondrial respiration (oxygen consumption rate, OCR) in SN homogenates form WT, D_1-*CB_1*-KO control mice, and CB_1 or DN22-CB_1 rescued in the striatonigral circuit (*see above **A and B***).

(**E)** Cataleptic effect of THC (10mg/kg i.p.) in WT, D_1-*CB_1*-KO control mice, and CB_1 or DN22-CB_1 rescued in the striatonigral circuit (*see above **A and B***).

(F) Effect of WIN (1µM) on mitochondrial respiration (oxygen consumption rate, OCR) in SN homogenates pre-treated with vehicle or the sAC blocker KH7 (5µM).

(**G and H)** Effects of intra-SNr administration of sAC blocker KH7 (2µg) on the **(G)** cataleptic, and **(H)** antinociceptive effect of systemic THC (10mg/kg i.p.) respect to vehicle treated mice.

(I) Effect of WIN (1µM) on mitochondrial respiration (oxygen consumption rate, OCR) in SN homogenates form D_1-Cre mice injected in the striatum with control (Ctr) virus or Cre-dependent mt-sAC expressing virus.

(J) Cataleptic, and **(K)** antinociceptive effects of systemic THC (10mg/kg i.p.) respect to vehicle in D_1-Cre mice injected with either control (Ctr) or Cre-dependent mt-sAC expressing virus in the striatum.

(L) Cataleptic, and **(M)** antinociceptive effect of systemic THC (10mg/kg i.p.) respect to vehicle in D_1-Cre mice injected with either control (Ctr) or Cre-dependent PKA-CA or MLS-PKA-CA expressing virus in the striatum.

(N) Effect of WIN (1µm) on mitochondrial respiration (oxygen consumption rate, OCR) in SN homogenates from D_1-Cre mice injected in the striatum with control virus or Cre-dependent PKA-CA or MLS-PKA-CA vectors.

SUPPLEMENTARY FIGURE LEGENDS

Figure S1 (related to main Figure 1). Cannabinoid-induced antinociception, but not catalepsy, relies on activation of striatonigral pmCB$_1$ and regulation of Substance-P/NK$_1$ receptor activity.

(A) SNr correct (hit) and misplaced (no-hit) cannula placements verified by infusion of skyblue toluidine solution followed by brain slicing and neutral red counterstaining. Representative histological analysis (top) and schematic representations (bottom, “hit” green dots, “no-hit” red dots) of the injection sites in the SNr.

(B) Effects of correct “hit” and misplaced “no-hit” intra-SNr administration of the cell permeable CB$_1$ antagonist AM251 on the hypolocomotor effect of systemic THC (10mg/kg i.p.) respect to vehicle treated mice.

(C) Schematic for striatonigral or striatopallidal CB$_1$ receptor deletion and representative pictures of viral injection sites. Green signal, striatal (STR) expression of AAV-FRT-iCre-EGFP. Blue signal, AAV-retro-FLP-BLFP or AAV-retro-BLFP expression in the globus pallidus (GPe) or in the substantia nigra reticulata (SNr).

(D) Representative micrograph (left) and relative quantification (right) of CB$_1$/D$_1$ and CB$_1$/D$_2$ co-expressing cells in the striatum of mice with striatopallidal (ST-GP-*CB$_1$*-KO) or striatonigral (ST-SN-*CB$_1$*-KO) CB$_1$ receptor deletion compared to control littermates. ec: external capsule. ns: non–statistically different. Scale bar, 50µm.

(E) Hypolocomotor effect of systemic THC (10mg/kg i.p.) respect to vehicle in mice with striatopallidal (ST-GP-*CB_1*-KO) or striatonigral (ST-SN-*CB_1*-KO) CB_1 receptor deletion compared to control littermates.

(F-G) Effects of i.p. administration of the NK_1 receptor agonist GR73632 (75 μg/kg) on the cataleptic **(F)** and antinociceptive **(G)** effects of systemic THC (10mg/kg i.p.) respect to vehicle treated mice.

(H) Left: Schematics of the Substance-P (SP) "sniffer cell" system. Co-expression of human NK_1 receptor (hNK_1R) and GCaMP6s in HEK293T cells facilitates detection of SP-induced calcium increases reflected by increased GCaMP6s fluorescence. Center: fluorescence micrographs of representative SP "sniffer cells" co-expressing hNK_1R-mCherry and GCaMP6s, and line-scan fluorescence quantification indicating membrane localization of hNK_1R. Right: representative fluorescence micrographs and kinetic trace of SP "sniffer cells" at baseline (time=0s) and following stimulation with 10nM SP (time=180s) added to the perfusion chamber following a 60s baseline recording. Dose response to SP in the same settings (bottom right) quantified as the change in GCaMP6s fluorescence normalized to baseline fluorescence (ΔF/F0) with increasing doses of SP. The EC50 for "sniffer cells" to SP was 5.088nM.

(I) GCaMP6 response to different doses of SP in presence of NK_1R or in its absence, indicating the specificity of the "sniffer cell" response.

(J) Left: traces of GCaMP6 fluorescence variation (ΔF/F0) from sniffer cells expressing only GCaMP6 or both GCaMP6/NK_1R in the absence (Vehicle) and in the presence of the NK_1R blocker CP122721 (CP) when electrical stimulation (gray bars) of the striatonigral pathway is applied. Right: summary bar graphs

comparing means ± SE values of ΔF induced by electrical stimulation in all sniffer cells responding and imaged over the SNr in Vehicle and CP conditions

(K) GCaMP6 fluorescence changes (ΔF) after electrical stimulation in control condition, after vehicle and 5µM WIN on the same cells.

(L) Induction of calcium increase by SP in presence of 5µM WIN *in vitro*.

(M) Representative traces of light evoked inhibitory post-synaptic currents (oIPSCs) in the SNr of D_1-Cre mice injected in the striatum with rAAV-DIO-ChrmisonR as explained in **Figure 1L**. Note the presence of small oIPSCs induced by blue light application using during calcium imaging.

Figure S2 (related to main Figure 2). Functional localization of CB_1 receptors at mitochondrial membranes within the SNr.

(A) Immunogold detection of CB_1 receptor by electron microscopy in WT and *CB_1*-KO mice in SNr. White arrows, plasma membrane gold particles; pink arrows, mitochondrial gold particles; scale bar: 500 nm.

(B) Schematic representation of the strategy employed for the generation of DN22-*CB_1*-KI mouse line. LHA: left homology arm; RHA, right homology arm.

(C) Top left: qRT-PCR analysis of CB_1 mRNA in different brain regions from WT, DN22-*CB_1*-KI and *CB_1*-KO mice. AMY, amygdala; HYP, hypothalamus; STR, striatum; HPC, hippocampus; AON, anterior olfactory nucleus; PFC, prefrontal cortex. n.d., not detected Top right and bottom: immunofluorescence detection and representative images of CB_1 receptor in the brain of WT vs DN22-*CB_1*-KI mice (*CB_1*-KO mice are shown as antibody negative control). CA1, hippocampal region; SNr, substantia nigra pars reticulata; STR, striatum; MC, motor cortex; AON, anterior olfactory nucleus; PFC, prefrontal cortex; CRB, cerebellum.

(D) Immunogold detection of CB_1 receptor by electron microscopy in WT and DN22-*CB_1*-KI mice in SNr. White arrows, plasma membrane gold particles; pink arrows, mitochondrial gold particles; scale bar: 500 nm.

(E) Representative autoradiograms of brain sections from basal, 1 µM and 10 µM WIN-stimulated [^{35}S]GTPγS binding in WT mice.

(F) Relative quantification of WIN-mediated [^{35}S]GTPγS over basal level at 1µM (left) and 10µM (right) doses in WT and DN22-*CB_1*-KI mice. SNr, substantia nigra reticulata; STR, striatum; PFC, prefrontal cortex; OB, olfactory bulb; HYP,

hypothalamus; GPe, external globus pallidus; HPC, hippocampus; CB, cerebellum; BLA, basolateral amygdala; AON, anterior olfactory nucleus; NAC, nucleus accumbens.

(G) Representative autoradiograms of brain sections from WT, DN22-CB_1-KI and CB_1-KO mice incubated with [^{3H}] CP55.940.

(H) Relative quantification of bound [^{3H}] CP55.940 in WT, DN22-CB_1-KI and CB_1-KO slices. SNr, substantia nigra pars reticulata; STR, striatum; PFC, prefrontal cortex; OB, olfactory bulb; HYP, hypothalamus; GPe, external globus pallidus; HPC, hippocampus; CB, cerebellum; BLA, basolateral amygdala; AON, anterior olfactory nucleus; NAC, nucleus accumbens.

(I) Representative trace of mitochondrial respiration in a substantia nigra preparation from WT, DN22-CB_1-KI and CB_1-KO mice. Substrates are malate, pyruvate and glutamate. The inhibitory effect of WIN was observed when the respiration was coupled to ATP synthesis via the addition of Adenosine diphosphate (ADP, see **Table S1**).

Figure S3 (related to main Figure 3). MtCB$_1$ receptors and their signaling mediate the cataleptic effect of cannabinoids in the striatonigral circuits. **(A)** Body weight (top panel) and muscular strength (measured by grid suspension test, bottom panel) of WT and DN22-*CB$_1$*-KI mice.

(B) Daily home cage locomotor activity of WT and DN22-*CB$_1$*-KI mice. Grey box indicate the night phase.

(C) Daily voluntary wheel running of WT and DN22-*CB$_1$*-KI mice. Grey box indicate the night phase.

(D) Time course plot showing eIPSCs amplitude before and after 3s depolarization (-70 to 0 mV grey line) in hippocampal slices obtained from WT and DN22-*CB$_1$*-KI mice.

(E) Representative traces of eIPSCs before and after 3s depolarization (-70 to 0 mV) in WT and DN22-*CB$_1$*-KI mice and averaged reduction of eIPSCs amplitude respect to baseline recorded during 3 sweeps after depolarization.

(F) Average paired pulse ratio (PPR) after optogenetic stimulation of striatonigral terminals in WT and DN22-*CB$_1$*-KI mice.

(G) Traces of GCaMP6 fluorescence variation (ΔF/F0) from sniffer cells in the absence (Vehicle) and in the presence of WIN when electrical stimulation (gray bars) of the striatonigral pathway in slices from DN22-*CB$_1$*-KI mice is applied. Plots are from the same cells in both conditions. Right: summary bar graphs comparing means ± SEM values of ΔF/F0 induced by electrical stimulation in all

sniffer cells responding and imaged over the SNr in Vehicle and WIN conditions in DN22-*CB_1*-KI mice.

(H) Effects of intra-SNr administration of the cell impermeable CB_1 antagonist Hemopressin (Hp, 22ng) on the antinociceptive effect of systemic THC (10mg/kg i.p.) in DN22-*CB_1*-KI mice.

(I) Effects of i.p. administration of the NK_1 receptor agonist GR73632 (75 μg/kg) on the antinociceptive effect of systemic THC (10mg/kg i.p.) respect to vehicle in DN22-*CB_1*-KI mice.

(J) Correlation between CB_1 fluorescence intensity in SNr (X axis) and immobility in the bar test induced by THC (Y axis) in D_1-*CB_1*-KO mice injected with rAAV-DIO-CB_1 (black dots) or with rAAV-DIO-DN22-CB_1 (grey dots) in the striatum.

(K) Effect of WIN (1µM) on mitochondrial respiration (oxygen consumption rate, OCR) in SN homogenates pre-treated with vehicle or GR736321 (1µM).

(L) Representative immunofluorescence of the mitochondrial protein TOMM20 and HA in Hela cells expressing pcDNA or mt-sAC. Scale bar: 10 µm.

(M) Representative pictures of HA-tag immunostaining in the dorsal striatum of D_1-Cre mice injected with control or Cre-dependent mt-sAC AAV. Scale bar 100µm.

(N) Western blotting for HA-tag, endogenous sAC, tubulin and Tomm20 after immuno-magnetic isolation of striatal mitochondria (Mito) compared to total cell

lysate (TCL) from D_1-Cre mice injected with control or Cre-dependent mt-sAC AAV in the dorsal striatum.

(O) Western blotting for HA-tag and endogenous sAC in SN homogenates (used for mitochondrial respiration, see **Figure 4I**) from D_1-Cre mice injected with control or Cre-dependent mt-sAC AAV in the dorsal striatum.

(P) Representative immunofluorescence and co-localization analysis of the mitochondrial protein TOMM20 and Myc in Hela cells expressing pcDNA, PKA-CA or MLS-PKA-CA. Scale bar: 10 µm. And Trypsin sensitivity assay (right).

(Q) Western blotting for Myc-tag, endogenous PKA, tubulin and Tomm20 after immuno-magnetic isolation of striatal mitochondria (Mito) compared to total cell lysate (TCL) from D_1-Cre mice injected with control or Cre-dependent PKA-CA or MLS-PKA-CA AAVs in the dorsal striatum.

(R) Western blotting for myc-tag in SN homogenates (used for mitochondrial respiration, see **Figure 4N**) from D_1-Cre mice injected with control or Cre-dependent PKA-CA or MLS-PKA-CA AAVs in the dorsal striatum.

Figure S4. Proposed mechanisms for the subcellular specificity of behavior control by CB_1 receptors in striatonigral circuits.

At striatonigral terminals, activation of pmCB1 triggers inhibition of cytosolic PKA, which in turn results in a reduction of Substance-P release and subsequent decrease of pain perception. In the same terminals, activation of $mtCB_1$ is responsible of motor impairment, by decreasing the release of GABA on SNr neurons trough inhibition of mitochondrial activity.

Table S1. Characterization of Mitochondrial respiration in SN extracts

CI_L, ComplexI Leak; CI_P, ComplexI OXPHOS; CI & CII_P, ComplexI and ComplexII OXPHOS; CII_P, ComplexII OXPHOS; ROX, Residual Oxigen Consumption.

Table S2. Statistical analysis. Related to Figure 1-4.

Table S3. Statistical analysis. Related to Figure S1-S3.

REFERENCES

Bellocchio, L., Lafenetre, P., Cannich, A., Cota, D., Puente, N., Grandes, P., Chaouloff, F., Piazza, P., and Marsicano, G. (2010). Bimodal control of stimulated food intake by the endocannabinoid system. Nature Neuroscience 13, 281–283.

Bellocchio, L., Ruiz-Calvo, A., Chiarlone, A., Cabanas, M., Resel, E., Cazalets, J.R., Blazquez, C., Cho, Y.H., Galve-Roperh, I., and Guzman, M. (2016). Sustained Gq-Protein Signaling Disrupts Striatal Circuits via JNK. The Journal of neuroscience : the official journal of the Society for Neuroscience 36, 10611-10624.

Benard, G., Massa, F., Puente, N., Lourenco, J., Bellocchio, L., Soria-Gomez, E., Matias, I., Delamarre, A., Metna-Laurent, M., Cannich, A.*, et al.* (2012). Mitochondrial CB(1) receptors regulate neuronal energy metabolism. Nature neuroscience 15, 558-564.

Boccella, S., Marabese, I., Guida, F., Luongo, L., Maione, S., and Palazzo, E. (2020). The Modulation of Pain by Metabotropic Glutamate Receptors 7 and 8 in the Dorsal Striatum. Curr Neuropharmacol 18, 34-50.

Borgelt, L.M., Franson, K.L., Nussbaum, A.M., and Wang, G.S. (2013). The pharmacologic and clinical effects of medical cannabis. Pharmacotherapy 33, 195-209.

Borgkvist, A., and Fisone, G. (2007). Psychoactive drugs and regulation of the cAMP/PKA/DARPP-32 cascade in striatal medium spiny neurons. Neuroscience and biobehavioral reviews 31, 79-88.

Borsook, D., Upadhyay, J., Chudler, E.H., and Becerra, L. (2010). A key role of the basal ganglia in pain and analgesia--insights gained through human functional imaging. Mol Pain 6, 27.

Bradford, M.M. (1976). A rapid and sensitive method for the quantitation of microgram quantities of protein utilizing the principle of protein-dye binding. Analytical Biochemistry 72, 248–254.

Brown, R.E. (2019). Review of Franz Joseph Gall: Naturalist of the mind, visionary of the brain. Hist Psychol 22, 374-379.

Bucko, P.J., Lombard, C.K., Rathbun, L., Garcia, I., Bhat, A., Wordeman, L., Smith, F.D., Maly, D.J., Hehnly, H., and Scott, J.D. (2019). Subcellular drug targeting illuminates local kinase action. Elife 8.

Busquets-Garcia, A., Bains, J., and Marsicano, G. (2018). CB1 Receptor Signaling in the Brain: Extracting Specificity from Ubiquity. Neuropsychopharmacology : official publication of the American College of Neuropsychopharmacology 43, 4-20.

Chazalon, M., Paredes-Rodriguez, E., Morin, S., Martinez, A., Cristovao-Ferreira, S., Vaz, S., Sebastiao, A., Panatier, A., Boue-Grabot, E., Miguelez, C., and Baufreton, J. (2018). GAT-3 Dysfunction Generates Tonic Inhibition in External Globus Pallidus Neurons in Parkinsonian Rodents. Cell Rep 23, 1678-1690.

Chen, W., Ennes, H.S., McRoberts, J.A., and Marvizon, J.C. (2018). Mechanisms of mu-opioid receptor inhibition of NMDA receptor-induced substance P release in the rat spinal cord. Neuropharmacology 128, 255-268.

Chomczynski, P., and Sacchi, N. (1987). Single-step method of RNA isolation by acid guanidinium thiocyanate-phenol-chloroform extraction. Anal Biochem 162, 156-159.

Choo, Y.S. (2004). Mutant huntingtin directly increases susceptibility of mitochondria to the calcium-induced permeability transition and cytochrome c release. Human Molecular Genetics 13, 1407–1420.

Clapper, J.R., Moreno-Sanz, G., Russo, R., Guijarro, A., Vacondio, F., Duranti, A., Tontini, A., Sanchini, S., Sciolino, N.R., Spradley, J.M., et al. (2010). Anandamide suppresses pain initiation through a peripheral endocannabinoid mechanism. Nat Neurosci 13, 1265–1270.

Cohen, K., Weizman, A., and Weinstein, A. (2019). Positive and Negative Effects of Cannabis and Cannabinoids on Health. Clin Pharmacol Ther 105, 1139-1147.

Creighton, J. (2011). Targeting therapeutic effects: subcellular location matters. Focus on "Pharmacological AMP-kinase activators have compartment-specific effects on cell physiology". Am J Physiol Cell Physiol 301, C1293-1295.

Darmani, N.A., and Pandya, D.K. (2000). Involvement of other neurotransmitters in behaviors induced by the cannabinoid CB1 receptor antagonist SR 141716A in naive mice. J Neural Transm (Vienna) 107, 931-945.

Deniau, J.M., Mailly, P., Maurice, N., and Charpier, S. (2007). The pars reticulata of the substantia nigra: a window to basal ganglia output. Progress in brain research 160, 151-172.

Donvito, G., Nass, S.R., Wilkerson, J.L., Curry, Z.A., Schurman, L.D., Kinsey, S.G., and Lichtman, A.H. (2018). The Endogenous Cannabinoid System: A Budding Source of Targets for Treating Inflammatory and Neuropathic Pain.

Neuropsychopharmacology : official publication of the American College of Neuropsychopharmacology 43, 52-79.

Dubreucq, S., Koehl, M., Abrous, D.N., Marsicano, G., and Chaouloff, F. (2010). CB1 receptor deficiency decreases wheel-running activity: consequences on emotional behaviours and hippocampal neurogenesis. Exp Neurol 224, 106-113.

Dwivedi, Y., and Pandey, G.N. (2008). Adenylyl cyclase-cyclicAMP signaling in mood disorders: role of the crucial phosphorylating enzyme protein kinase A. Neuropsychiatr Dis Treat 4, 161-176.

Eichel, K., and von Zastrow, M. (2018). Subcellular Organization of GPCR Signaling. Trends Pharmacol Sci 39, 200-208.

Fernandez-Ruiz, J., Moreno-Martet, M., Rodriguez-Cueto, C., Palomo-Garo, C., Gomez-Canas, M., Valdeolivas, S., Guaza, C., Romero, J., Guzman, M., Mechoulam, R., and Ramos, J.A. (2011). Prospects for cannabinoid therapies in basal ganglia disorders. Br J Pharmacol 163, 1365-1378.

Francisco, A., Engel, D.F., Figueira, T.R., Rogerio, F., de Bem, A.F., and Castilho, R.F. (2020). Mitochondrial NAD(P)(+) Transhydrogenase is Unevenly Distributed in Different Brain Regions, and its Loss Causes Depressive-like Behavior and Motor Dysfunction in Mice. Neuroscience 440, 210-229.

Freeze, B.S., Kravitz, A.V., Hammack, N., Berke, J.D., and Kreitzer, A.C. (2013). Control of basal ganglia output by direct and indirect pathway projection neurons. The Journal of neuroscience : the official journal of the Society for Neuroscience 33, 18531-18539.

Garcia, C., Palomo-Garo, C., Gomez-Galvez, Y., and Fernandez-Ruiz, J. (2016). Cannabinoid-dopamine interactions in the physiology and physiopathology of the basal ganglia. Br J Pharmacol 173, 2069-2079.

Garcia, G.C., Bartol, T.M., Phan, S., Bushong, E.A., Perkins, G., Sejnowski, T.J., Ellisman, M.H., and Skupin, A. (2019). Mitochondrial morphology provides a mechanism for energy buffering at synapses. Sci Rep 9, 18306.

Giuffrida, A., and Seillier, A. (2012). New insights on endocannabinoid transmission in psychomotor disorders. Prog Neuropsychopharmacol Biol Psychiatry 38, 51-58.

Griebel, G., Stemmelin, J., and Scatton, B. (2005). Effects of the cannabinoid CB1 receptor antagonist rimonabant in models of emotional reactivity in rodents. Biological Psychiatry 57, 261–267.

Guedouari, H., Daigle, T., Scorrano, L., and Hebert-Chatelain, E. (2017). Sirtuin 5 protects mitochondria from fragmentation and degradation during starvation. Biochimica et Biophysica Acta (BBA) - Molecular Cell Research 1864, 169–176.

Gutierrez-Rodriguez, A., Bonilla-Del Rio, I., Puente, N., Gomez-Urquijo, S.M., Fontaine, C.J., Egana-Huguet, J., Elezgarai, I., Ruehle, S., Lutz, B., Robin, L.M.*, et al.* (2018). Localization of the cannabinoid type-1 receptor in subcellular astrocyte compartments of mutant mouse hippocampus. Glia 66, 1417-1431.

Häring, M., Kaiser, N., Monory, K., and Lutz, B. (2011). Circuit Specific Functions of Cannabinoid CB1 Receptor in the Balance of Investigatory Drive and Exploration. PLoS ONE 6, e26617.

Hebert-Chatelain, E., Desprez, T., Serrat, R., Bellocchio, L., Soria-Gomez, E., Busquets-Garcia, A., Pagano Zottola, A.C., Delamarre, A., Cannich, A., Vincent,

P.*, et al.* (2016). A cannabinoid link between mitochondria and memory. Nature 539, 555-559.

Heimann, A.S., Gomes, I., Dale, C.S., Pagano, R.L., Gupta, A., de Souza, L.L., Luchessi, A.D., Castro, L.M., Giorgi, R., Rioli, V.*, et al.* (2007). Hemopressin is an inverse agonist of CB1 cannabinoid receptors. Proceedings of the National Academy of Sciences of the United States of America 104, 20588-20593.

Ibsen, M.S., Connor, M., and Glass, M. (2017). Cannabinoid CB1 and CB2 Receptor Signaling and Bias. Cannabis Cannabinoid Res 2, 48-60.

Ilouz, R., Lev-Ram, V., Bushong, E.A., Stiles, T.L., Friedmann-Morvinski, D., Douglas, C., Goldberg, J.L., Ellisman, M.H., and Taylor, S.S. (2017). Isoform-specific subcellular localization and function of protein kinase A identified by mosaic imaging of mouse brain. Elife 6.

Jimenez-Blasco, D., Busquets-Garcia, A., Hebert-Chatelain, E., Serrat, R., Vicente-Gutierrez, C., Ioannidou, C., Gomez-Sotres, P., Lopez-Fabuel, I., Resch-Beusher, M., Resel, E., et al. (2020). Glucose metabolism links astroglial mitochondria to cannabinoid effects. Nature 583, 603-608.

Johnson, M.B., Young, A.D., and Marriott, I. (2016). The Therapeutic Potential of Targeting Substance P/NK-1R Interactions in Inflammatory CNS Disorders. Front Cell Neurosci 10, 296.

Kanellopoulos, A.K., Mariano, V., Spinazzi, M., Woo, Y.J., McLean, C., Pech, U., Li, K.W., Armstrong, J.D., Giangrande, A., Callaerts, P.*, et al.* (2020). Aralar Sequesters GABA into Hyperactive Mitochondria, Causing Social Behavior Deficits. Cell 180, 1178-1197 e1120.

Kano, M., Ohno-Shosaku, T., Hashimotodani, Y., Uchigashima, M., and Watanabe, M. (2009). Endocannabinoid-mediated control of synaptic transmission. Physiol Rev 89, 309–380.

Klapoetke, N.C., Murata, Y., Kim, S.S., Pulver, S.R., Birdsey-Benson, A., Cho, Y.K., Morimoto, T.K., Chuong, A.S., Carpenter, E.J., Tian, Z., et al. (2014). Independent optical excitation of distinct neural populations. Nat Methods 11, 338–346.

Knight, R.T. (2007). Neuroscience. Neural networks debunk phrenology. Science 316, 1578-1579.

Koch, M., Varela, L., Kim, J.G., Kim, J.D., Hernandez-Nuno, F., Simonds, S.E., Castorena, C.M., Vianna, C.R., Elmquist, J.K., Morozov, Y.M., et al. (2015). Hypothalamic POMC neurons promote cannabinoid-induced feeding. Nature 519, 45–50.

Lahuna, O., and Jockers, R. (2018). [Mitochondrial signaling of G protein-coupled receptors]. Biol Aujourdhui 212, 21-26.

Lemberger, T., Parlato, R., Dassesse, D., Westphal, M., Casanova, E., Turiault, M., Tronche, F., Schiffmann, S.N., and Schutz, G. (2007). Expression of Cre recombinase in dopaminoceptive neurons. BMC Neurosci 8, 4.

Lever, I.J., and Malcangio, M. (2002). CB(1) receptor antagonist SR141716A increases capsaicin-evoked release of Substance P from the adult mouse spinal cord. Br J Pharmacol 135, 21-24.

Livak, K.J., and Schmittgen, T.D. (2001). Analysis of relative gene expression data using real-time quantitative PCR and the 2(-Delta Delta C(T)) Method. Methods 25, 402-408.

Makrecka-Kuka, M., Krumschnabel, G., and Gnaiger, E. (2015). High-Resolution Respirometry for Simultaneous Measurement of Oxygen and Hydrogen Peroxide Fluxes in Permeabilized Cells, Tissue Homogenate and Isolated Mitochondria. Biomolecules 5, 1319-1338.

Marsicano, G., Goodenough, S., Monory, K., Hermann, H., Eder, M., Cannich, A., Azad, S.C., Cascio, M.G., Gutierrez, S.O., van der Stelt, M.*, et al.* (2003). CB1 cannabinoid receptors and on-demand defense against excitotoxicity. Science 302, 84-88.

Marsicano, G., and Kuner, R. (2008). Anatomical distribution of receptors, ligands and enzymes in the brain and the spinal cord: circuitries and neurochemistry. In Cannabinoids and the brain, A. Kofalvi, ed. (New York: Springer), pp. 161-202.

Martin, J.L., Gadegbeku, B., Wu, D., Viallon, V., and Laumon, B. (2017). Cannabis, alcohol and fatal road accidents. PloS one 12, e0187320.

Martinez, A., Macheda, T., Morgese, M.G., Trabace, L., and Giuffrida, A. (2012). The cannabinoid agonist WIN55212-2 decreases L-DOPA-induced PKA activation and dyskinetic behavior in 6-OHDA-treated rats. Neurosci Res 72, 236-242.

Metna-Laurent, M., Mondesir, M., Grel, A., Vallee, M., and Piazza, P.V. (2017). Cannabinoid-Induced Tetrad in Mice. Curr Protoc Neurosci 80, 9 59 51-59 59 10.

Monory, K., Blaudzun, H., Massa, F., Kaiser, N., Lemberger, T., Schutz, G., Wotjak, C.T., Lutz, B., and Marsicano, G. (2007). Genetic dissection of behavioural and autonomic effects of Delta(9)-tetrahydrocannabinol in mice. PLoS biology 5, e269.

Nadal, X., La Porta, C., Andreea Bura, S., and Maldonado, R. (2013). Involvement of the opioid and cannabinoid systems in pain control: New insights from knockout studies. European Journal of Pharmacology 716, 142–157.

Niswender, C.M., Willis, B.S., Wallen, A., Sweet, I.R., Jetton, T.L., Thompson, B.R., Wu, C., Lange, A.J., and McKnight, G.S. (2005). Cre recombinase-dependent expression of a constitutively active mutant allele of the catalytic subunit of protein kinase A. Genesis 43, 109-119.

Oliveira da Cruz, J., Busquets-Garcia, A., Zhao, Z., Varilh, M., Lavanco, G., Bellocchio, L., Robin, L., Cannich, A., Julio-Kalajzić, F., Lesté-Laserre,T., Maitre, M., Drago, F., Marsicano, G., Soria-Gomez, E. (2020). Specific Hippocampal Interneurons Shape Consolidation of Recognition Memory. Cell Reports. 32(7): 108046. doi: 10.1016/j.celrep.2020.108046

Oshita, K., Inoue, A., Tang, H.B., Nakata, Y., Kawamoto, M., and Yuge, O. (2005). CB(1) cannabinoid receptor stimulation modulates transient receptor potential vanilloid receptor 1 activities in calcium influx and substance P Release in cultured rat dorsal root ganglion cells. J Pharmacol Sci 97, 377-385.

Pagano Zottola , A.C., Soria-Gomez, E., Bonilla-del-Río, I., Muguruza, C., Terral, G., Robin, L.M., Oliveira da Cruz, J.F., Redon, B., Lesté-Lasserre, T., Tolentino-Cortes, T Puente, N., Barreda-Gómez, G Chaouloff, F., Callado, L.F., Grandes, P., Marsicano, G., Bellocchio, L. (2020). A new mutant mouse model lacking mitochondrial-associated CB1 receptor. Biorxiv.

Pautrat, A., Rolland, M., Barthelemy, M., Baunez, C., Sinniger, V., Piallat, B., Savasta, M., Overton, P.G., David, O., and Coizet, V. (2018). Revealing a novel

nociceptive network that links the subthalamic nucleus to pain processing. ELife 7, e36607.

Paxinos, G., and Franklin, K.B.J. (2001). The Mouse Brain in Stereotaxic Coordinates (S. Diego (USA): Academic Press).

Pertwee, R.G. (2001). Cannabinoid receptors and pain. Progress in neurobiology 63, 569-611.

Prashad, S., and Filbey, F.M. (2017). Cognitive motor deficits in cannabis users. Curr Opin Behav Sci 13, 1-7.

Puente, N., Bonilla-Del Río, I., Achicallende, S., Nahirney, P.C., and Grandes, P. (2019). High-resolution Immunoelectron Microscopy Techniques for Revealing Distinct Subcellular Type 1 Cannabinoid Receptor Domains in Brain. Bioprotocol 9.

Qi, G., Mi, Y., and Yin, F. (2019). Cellular Specificity and Inter-cellular Coordination in the Brain Bioenergetic System: Implications for Aging and Neurodegeneration. Front Physiol 10, 1531.

Rajendran, L., Knolker, H.J., and Simons, K. (2010). Subcellular targeting strategies for drug design and delivery. Nat Rev Drug Discov 9, 29-42.

Rangaraju, V., Calloway, N., and Ryan, T.A. (2014). Activity-driven local ATP synthesis is required for synaptic function. Cell 156, 825-835.

Ray, A.P., Chebolu, S., Ramirez, J., and Darmani, N.A. (2009). Ablation of least shrew central neurokinin NK1 receptors reduces GR73632-induced vomiting. Behavioral neuroscience 123, 701-706.

Redon, B., Violleau, C., Georges, F., Marsicano, G., and Chaouloff, F. (2020). The ergogenic impact of the glucocorticoid prednisolone does not translate into increased running motivation in mice. Psychoneuroendocrinology 111, 104489.

Rozenfeld, R., and Devi, L.A. (2008). Regulation of CB1 cannabinoid receptor trafficking by the adaptor protein AP-3. FASEB journal : official publication of the Federation of American Societies for Experimental Biology 22, 2311-2322.

Ruehle, S., Remmers, F., Romo-Parra, H., Massa, F., Wickert, M., Wortge, S., Haring, M., Kaiser, N., Marsicano, G., Pape, H.C., and Lutz, B. (2013). Cannabinoid CB1 Receptor in Dorsal Telencephalic Glutamatergic Neurons: Distinctive Sufficiency for Hippocampus-Dependent and Amygdala-Dependent Synaptic and Behavioral Functions. The Journal of neuroscience : the official journal of the Society for Neuroscience 33, 10264-10277.

Sales-Carbonell, C., Rueda-Orozco, P.E., Soria-Gomez, E., Buzsaki, G., Marsicano, G., and Robbe, D. (2013). Striatal GABAergic and cortical glutamatergic neurons mediate contrasting effects of cannabinoids on cortical network synchrony. Proceedings of the National Academy of Sciences of the United States of America 110, 719-724.

Simpson, D. (2005). Phrenology and the neurosciences: contributions of F. J. Gall and J. G. Spurzheim. ANZ J Surg 75, 475-482.

Skalhegg, B.S., and Tasken, K. (2000). Specificity in the cAMP/PKA signaling pathway. Differential expression,regulation, and subcellular localization of subunits of PKA. Front Biosci 5, D678-693.

Soria-Gomez, E., Bellocchio, L., Reguero, L., Lepousez, G., Martin, C., Bendahmane, M., Ruehle, S., Remmers, F., Desprez, T., Matias, I.*, et al.* (2014). The endocannabinoid system controls food intake via olfactory processes. Nature neuroscience 17, 407-415.

Steiner, H., Bonner, T.I., Zimmer, A.M., Kitai, S.T., and Zimmer, A. (1999). Altered gene expression in striatal projection neurons in CB1 cannabinoid

receptor knockout mice. Proceedings of the National Academy of Sciences of the United States of America 96, 5786-5790.

Steinhoff, M.S., von Mentzer, B., Geppetti, P., Pothoulakis, C., and Bunnett, N.W. (2014). Tachykinins and their receptors: contributions to physiological control and the mechanisms of disease. Physiol Rev 94, 265-301.

Szabo, B., Wallmichrath, I., Mathonia, P., and Pfreundtner, C. (2000). Cannabinoids inhibit excitatory neurotransmission in the substantia nigra pars reticulata. Neuroscience 97, 89-97.

Taylor, A.M., Becker, S., Schweinhardt, P., and Cahill, C. (2016). Mesolimbic dopamine signaling in acute and chronic pain: implications for motivation, analgesia, and addiction. Pain 157, 1194-1198.

Terral, G., Busquets-Garcia, A., Varilh, M., Achicallende, S., Cannich, A., Bellocchio, L., Bonilla-Del Río, I., Massa, F., Puente, N., Soria-Gomez, E., et al. (2019). CB1 Receptors in the Anterior Piriform Cortex Control Odor Preference Memory. Current Biology 29, 2455-2464.e5.

Vallee, M., Vitiello, S., Bellocchio, L., Hebert-Chatelain, E., Monlezun, S., Martin-Garcia, E., Kasanetz, F., Baillie, G.L., Panin, F., Cathala, A.*, et al.* (2014). Pregnenolone can protect the brain from cannabis intoxication. Science 343, 94-98.

Valsecchi, F., Konrad, C., and Manfredi, G. (2014). Role of soluble adenylyl cyclase in mitochondria. Biochim Biophys Acta 1842, 2555-2560.

Vos, M., Lauwers, E., and Verstreken, P. (2010). Synaptic mitochondria in synaptic transmission and organization of vesicle pools in health and disease. Front Synaptic Neurosci 2, 139.

Wilson, R.I., Kunos, G., and Nicoll, R.A. (2001). Presynaptic specificity of endocannabinoid signaling in the hippocampus. Neuron 31, 453-462.

Woodhams, S.G., Chapman, V., Finn, D.P., Hohmann, A.G., and Neugebauer, V. (2017). The cannabinoid system and pain. Neuropharmacology 124, 105-120.

Zaelzer, C., Gizowski, C., Salmon, C.K., Murai, K.K., and Bourque, C.W. (2018). Detection of activity-dependent vasopressin release from neuronal dendrites and axon terminals using sniffer cells. J Neurophysiol 120, 1386-1396.

Zhao, Z., Soria-Gomez, E., Varilh, M., Covelo, A., Julio-Kalajzic, F., Cannich, A., Castiglione, A., Vanhoutte, L., Duveau, A., Zizzari, P Beyeler, A., Cota, D., Bellocchio, L., Busquets-Garcia, A., Marsicano, G. (2020). A novel cortical mechanism for top-down control of water intake. Curr Biol 30, 4789-4798.

Zhou, F.M. (2016). The Substantia Nigra Pars Reticulata. In Handbook of Behavioral Neuroscience, (Elsevier), pp. 293–316.

Figure 1

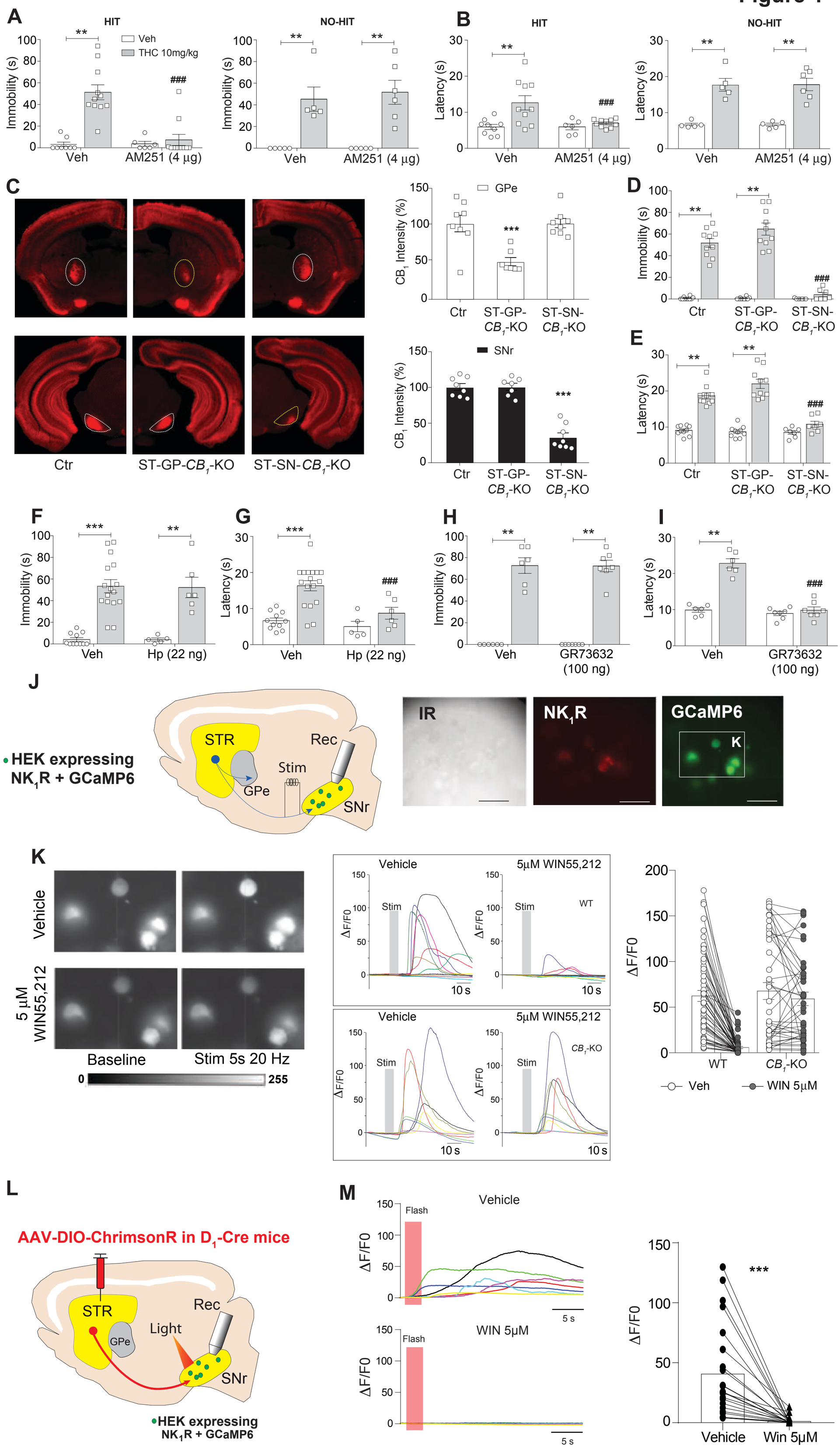
A
HIT
NO-HIT
Veh
THC 10mg/kg
Immobility (s)
Veh
AM251 (4 µg)
B
Latency (s)
C
Ctr
ST-GP-CB1-KO
ST-SN-CB1-KO
GPe
SNr
CB1 Intensity (%)
D
E
F
Hp (22 ng)
G
H
GR73632 (100 ng)
I
J
HEK expressing NK1R + GCaMP6
STR
Rec
Stim
GPe
SNr
IR
NK1R
GCaMP6
K
Vehicle
5 µM WIN55,212
Baseline
Stim 5s 20 Hz
5µM WIN55,212
Stim
10 s
WT
CB1-KO
ΔF/F0
Veh
WIN 5µM
L
AAV-DIO-ChrimsonR in D1-Cre mice
Light
M
Flash
WIN 5µM
5 s
Win 5µM

Figure 2

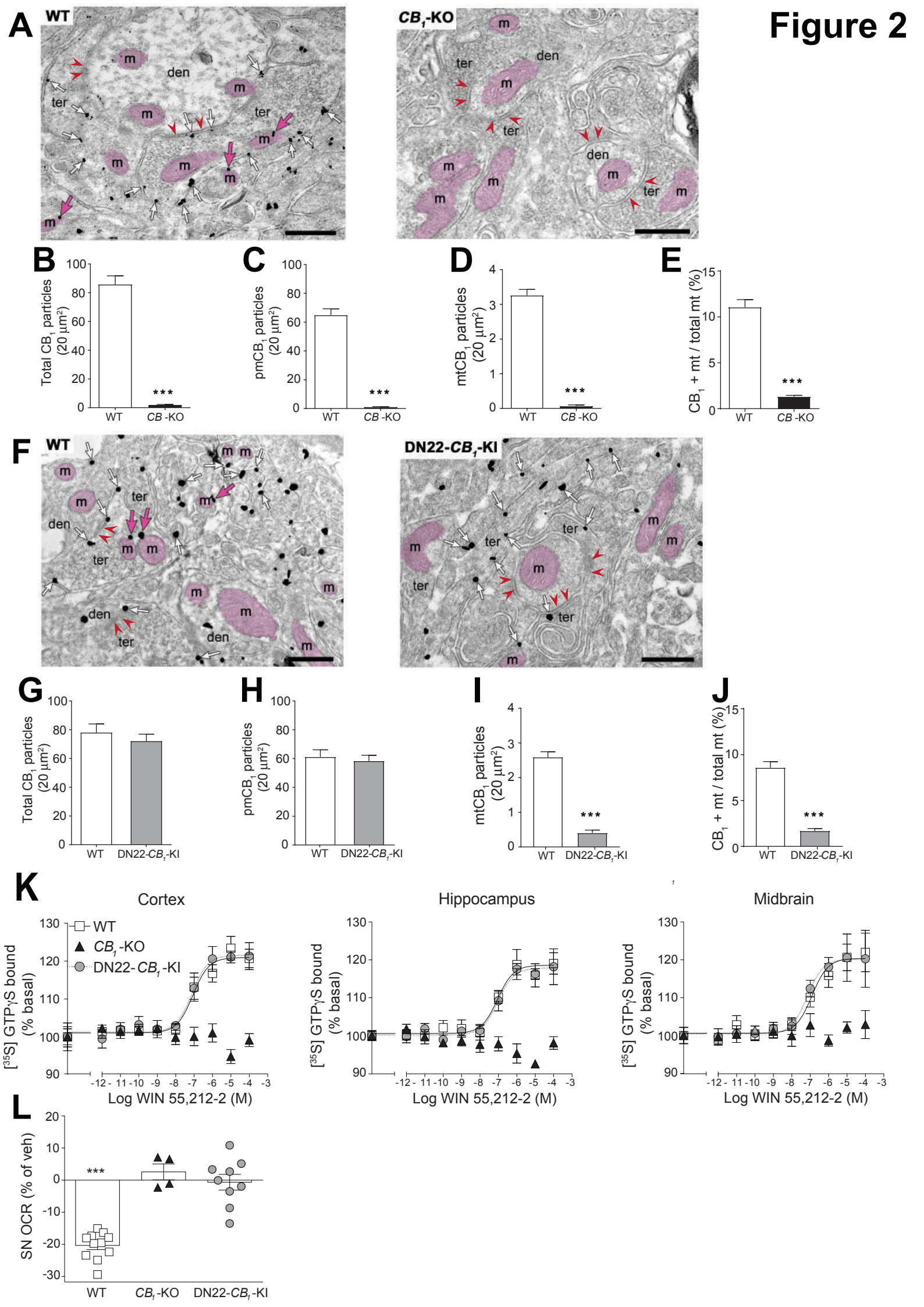
A
WT
CB1-KO
m
den
ter
B
Total CB1 particles (20 µm²)
WT
CB-KO
***
C
pmCB1 particles (20 µm²)
D
mtCB1 particles (20 µm²)
E
CB1 + mt / total mt (%)
F
DN22-CB1-KI
G
H
I
J
K
Cortex
Hippocampus
Midbrain
[35S] GTPγS bound (% basal)
Log WIN 55,212-2 (M)
L
SN OCR (% of veh)

Figure 3

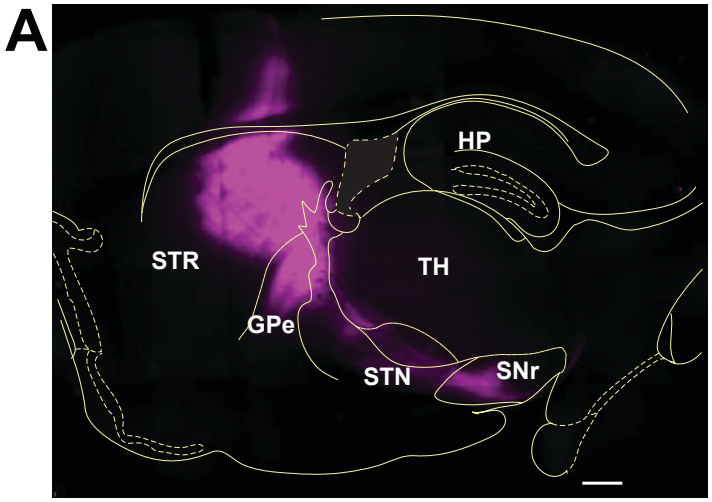
A
HP
STR
TH
GPe
STN
SNr

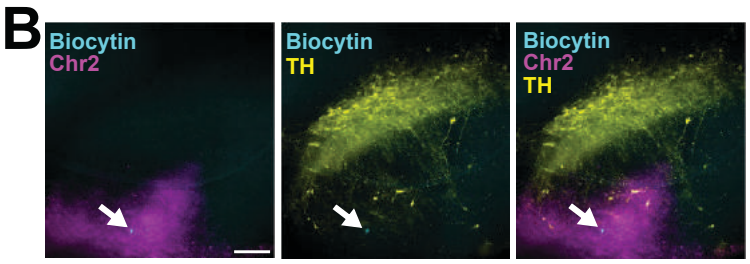
B
Biocytin
Chr2
Biocytin
TH
Biocytin
Chr2
TH

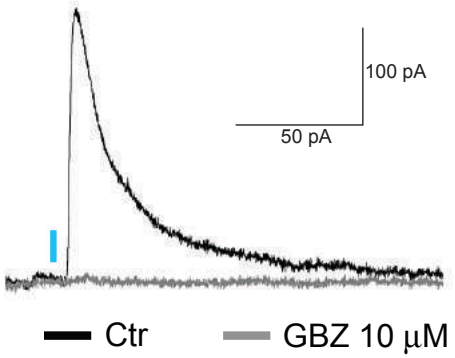
C
100 pA
50 pA
Ctr
GBZ 10 µM

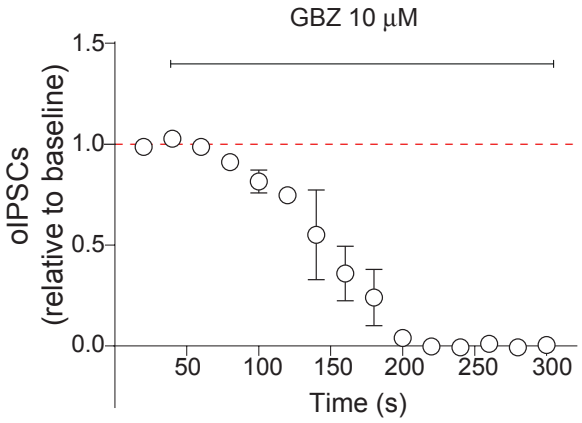
GBZ 10 µM
oIPSCs
(relative to baseline)
1.5
1.0
0.5
0.0
50
100
150
200
250
300
Time (s)

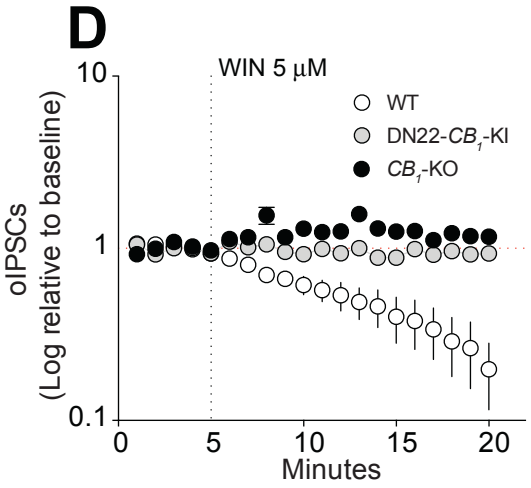
D
WIN 5 µM
WT
DN22-CB1-KI
CB1-KO
oIPSCs
(Log relative to baseline)
10
1
0.1
0
5
10
15
20
Minutes

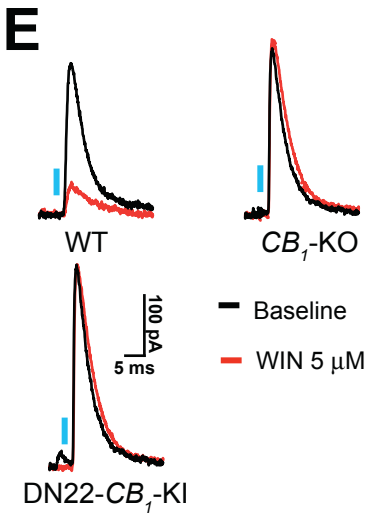
E
WT
CB1-KO
100 pA
5 ms
Baseline
WIN 5 µM
DN22-CB1-KI

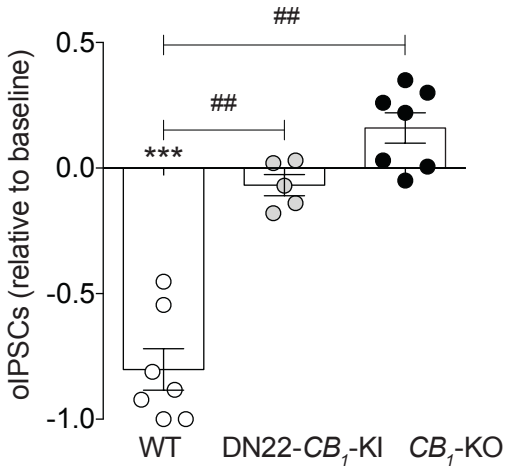
##
##
***
oIPSCs (relative to baseline)
0.5
0.0
-0.5
-1.0
WT
DN22-CB1-KI
CB1-KO

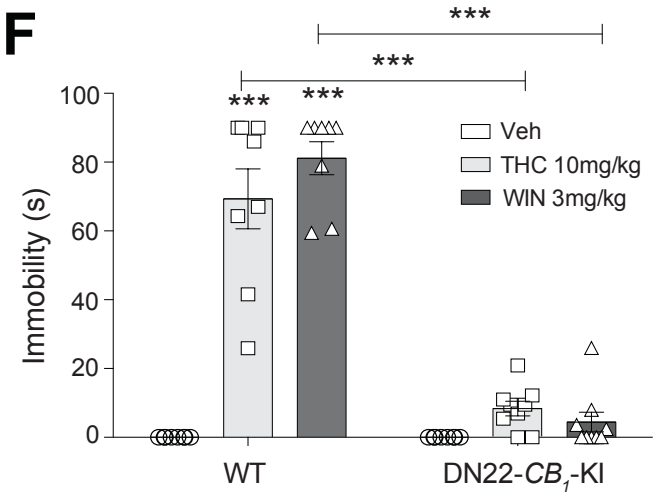
F
***
***
***
***
Immobility (s)
100
80
60
40
20
0
Veh
THC 10mg/kg
WIN 3mg/kg
WT
DN22-CB1-KI

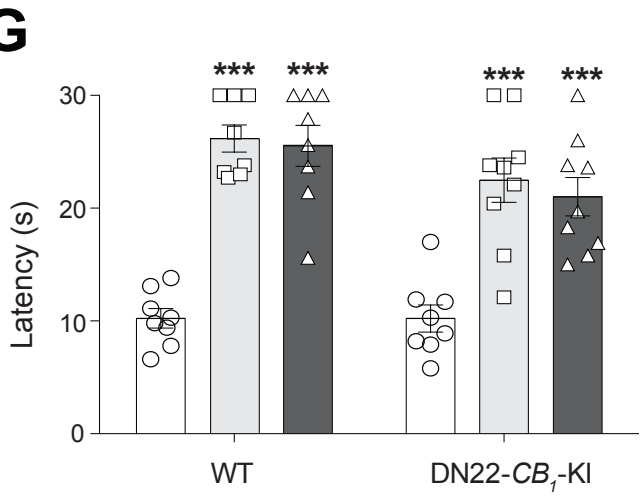
G
***
***
***
***
Latency (s)
30
20
10
0
WT
DN22-CB1-KI

Figure 4

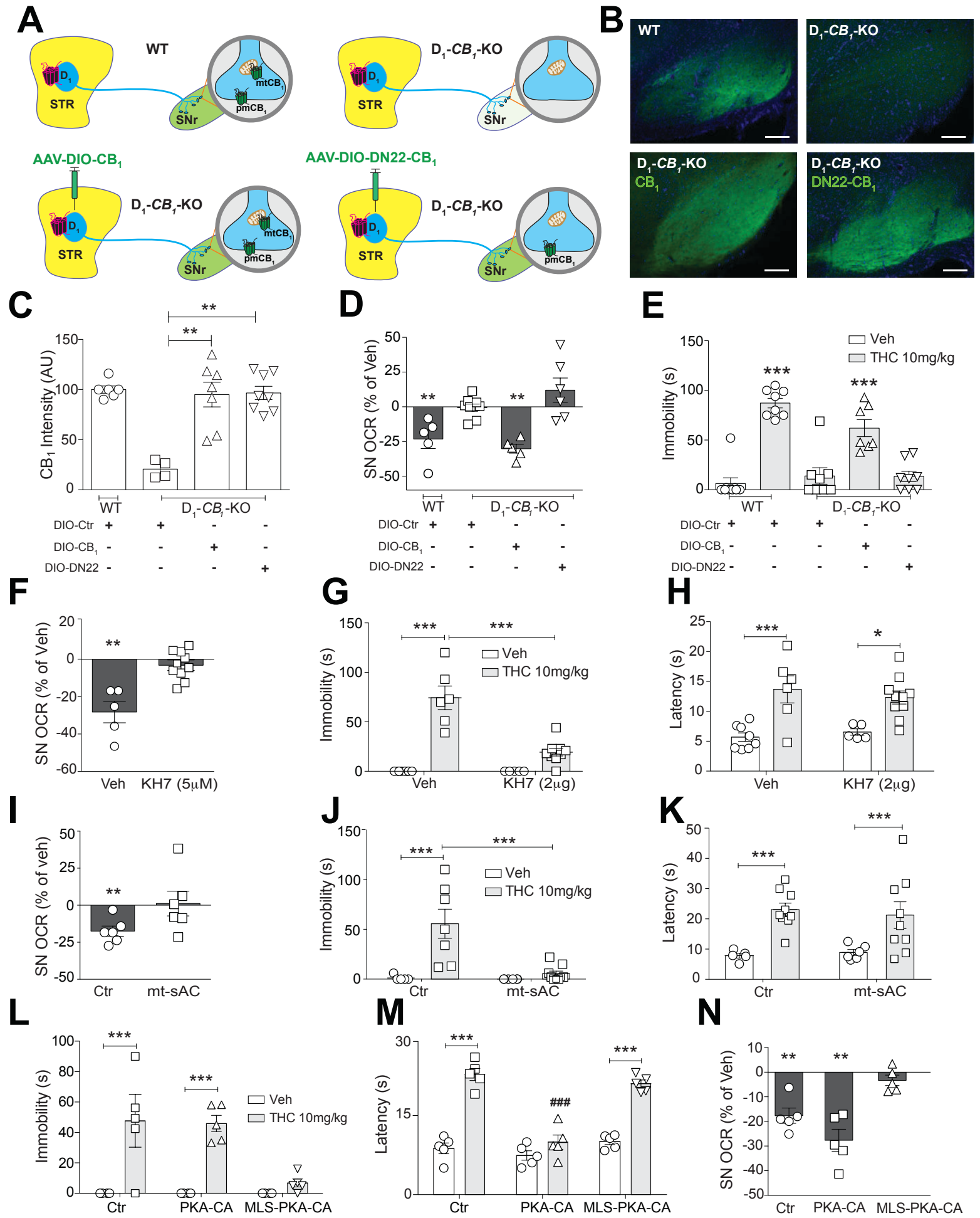
A
WT
D1-CB1-KO
STR
SNr
mtCB1
pmCB1
AAV-DIO-CB1
AAV-DIO-DN22-CB1
B
WT
D1-CB1-KO
CB1
DN22-CB1
C
CB1 Intensity (AU)
D
SN OCR (% of Veh)
E
Immobility (s)
Veh
THC 10mg/kg
DIO-Ctr
DIO-CB1
DIO-DN22
F
SN OCR (% of Veh)
Veh
KH7 (5μM)
G
Immobility (s)
KH7 (2μg)
H
Latency (s)
I
SN OCR (% of veh)
Ctr
mt-sAC
J
Immobility (s)
K
Latency (s)
L
Immobility (s)
PKA-CA
MLS-PKA-CA
M
Latency (s)
N
SN OCR (% of Veh)

Figure S1

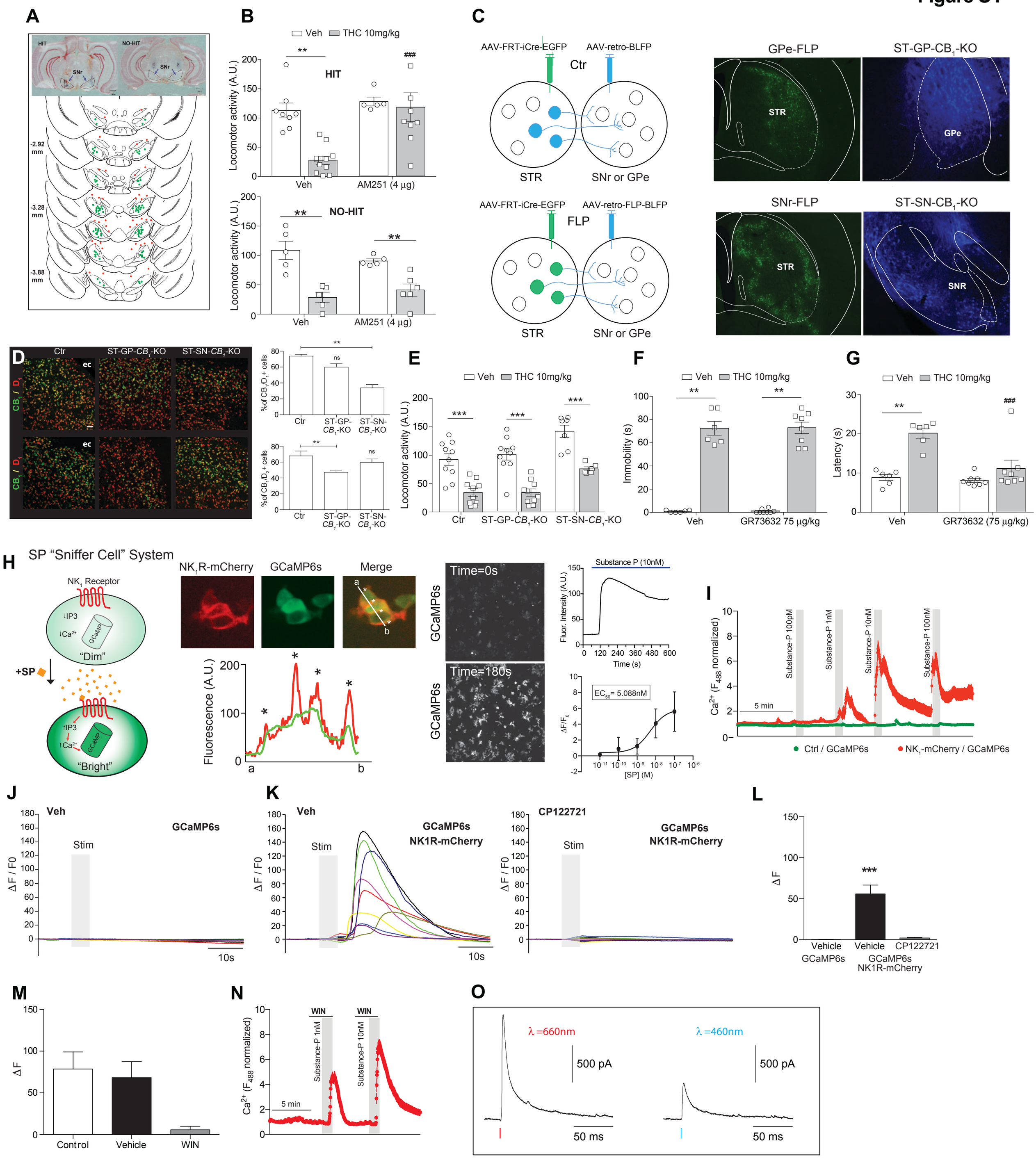
A
HIT
NO-HIT
SNr
-2.92 mm
-3.28 mm
-3.88 mm
B
Veh
THC 10mg/kg
HIT
NO-HIT
Locomotor activity (A.U.)
Veh
AM251 (4 µg)
C
AAV-FRT-iCre-EGFP
AAV-retro-BLFP
Ctr
STR
SNr or GPe
AAV-FRT-iCre-EGFP
AAV-retro-FLP-BLFP
FLP
GPe-FLP
ST-GP-CB1-KO
GPe
SNr-FLP
ST-SN-CB1-KO
SNR
D
Ctr
ST-GP-CB1-KO
ST-SN-CB1-KO
ec
CB1 / D1
CB1 / D2
%of CB1/D1+ cells
%of CB1/D2+ cells
ns
E
Veh
THC 10mg/kg
Locomotor activity (A.U.)
Ctr
ST-GP-CB1-KO
ST-SN-CB1-KO
F
Immobility (s)
Veh
GR73632 75 µg/kg
G
Latency (s)
GR73632 (75 µg/kg)
H
SP "Sniffer Cell" System
NK1 Receptor
↓IP3
↓Ca2+
GCaMP
"Dim"
+SP
↑IP3
↑Ca2+
"Bright"
NK1R-mCherry
GCaMP6s
Merge
Fluorescence (A.U.)
Time=0s
Time=180s
Substance P (10nM)
Fluor. Intensity (A.U.)
Time (s)
EC50= 5.088nM
ΔF/F0
[SP] (M)
I
Substance-P 100pM
Substance-P 1nM
Substance-P 10nM
Substance-P 100nM
5 min
Ca2+ (F488 normalized)
Ctrl / GCaMP6s
NK1-mCherry / GCaMP6s
J
Veh
GCaMP6s
Stim
ΔF / F0
10s
K
Veh
GCaMP6s
NK1R-mCherry
CP122721
L
ΔF
Vehicle
CP122721
GCaMP6s
NK1R-mCherry
M
Control
Vehicle
WIN
N
WIN
Substance-P 1nM
Substance-P 10nM
O
λ =660nm
λ =460nm
500 pA
50 ms

Figure S2

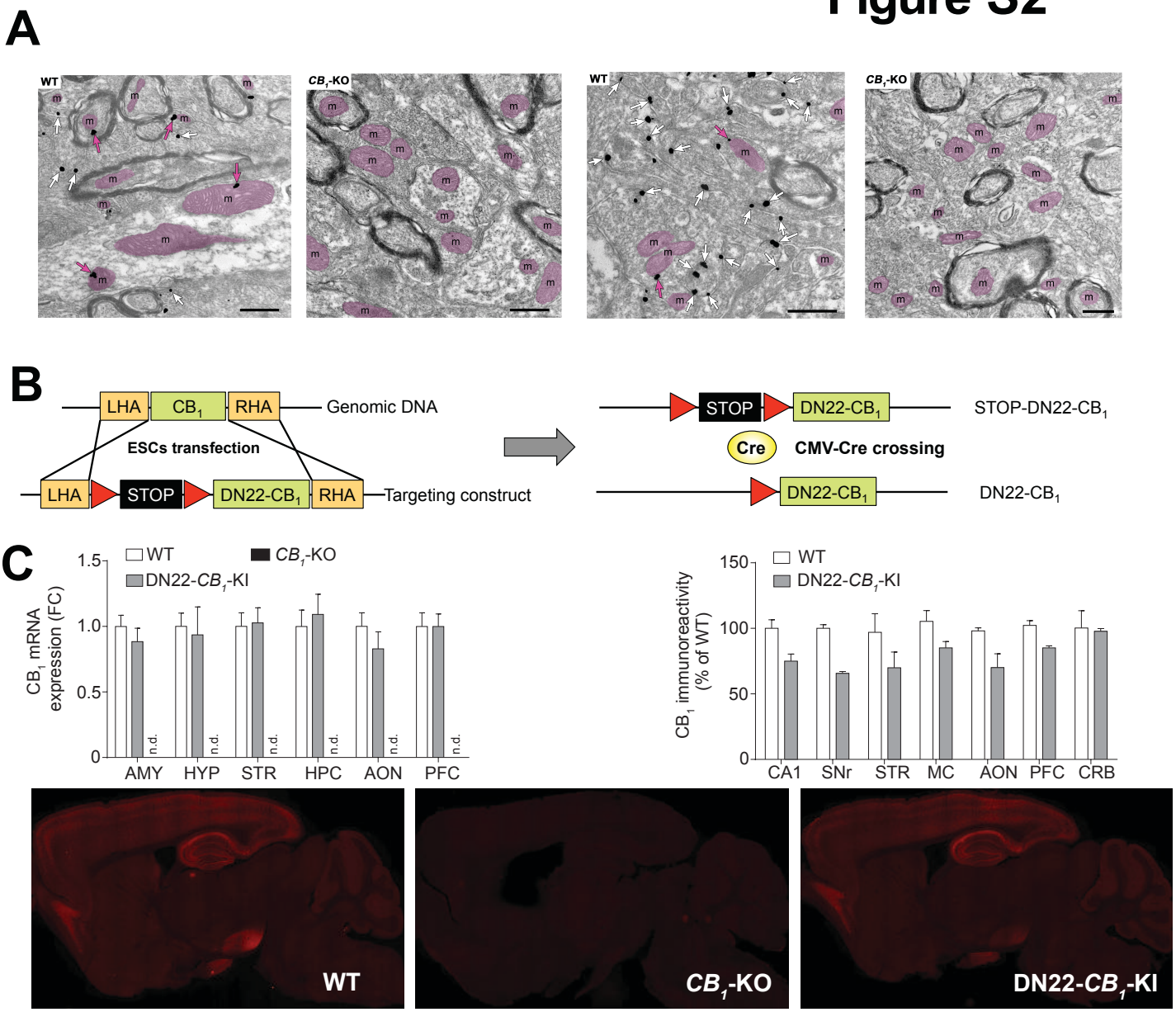
A
WT
CB1-KO
WT
CB1-KO
B
LHA
CB1
RHA
Genomic DNA
ESCs transfection
LHA
STOP
DN22-CB1
RHA
Targeting construct
STOP
DN22-CB1
STOP-DN22-CB1
Cre
CMV-Cre crossing
DN22-CB1
DN22-CB1
C
WT
CB1-KO
DN22-CB1-KI
CB1 mRNA expression (FC)
1.5
1.0
0.5
0
n.d.
AMY
HYP
STR
HPC
AON
PFC
WT
DN22-CB1-KI
CB1 immunoreactivity (% of WT)
150
100
50
0
CA1
SNr
STR
MC
AON
PFC
CRB
WT
CB1-KO
DN22-CB1-KI
D
WT
DN22-CB1-KI
WT
DN22-CB1-KI

Figure S2 (cont)

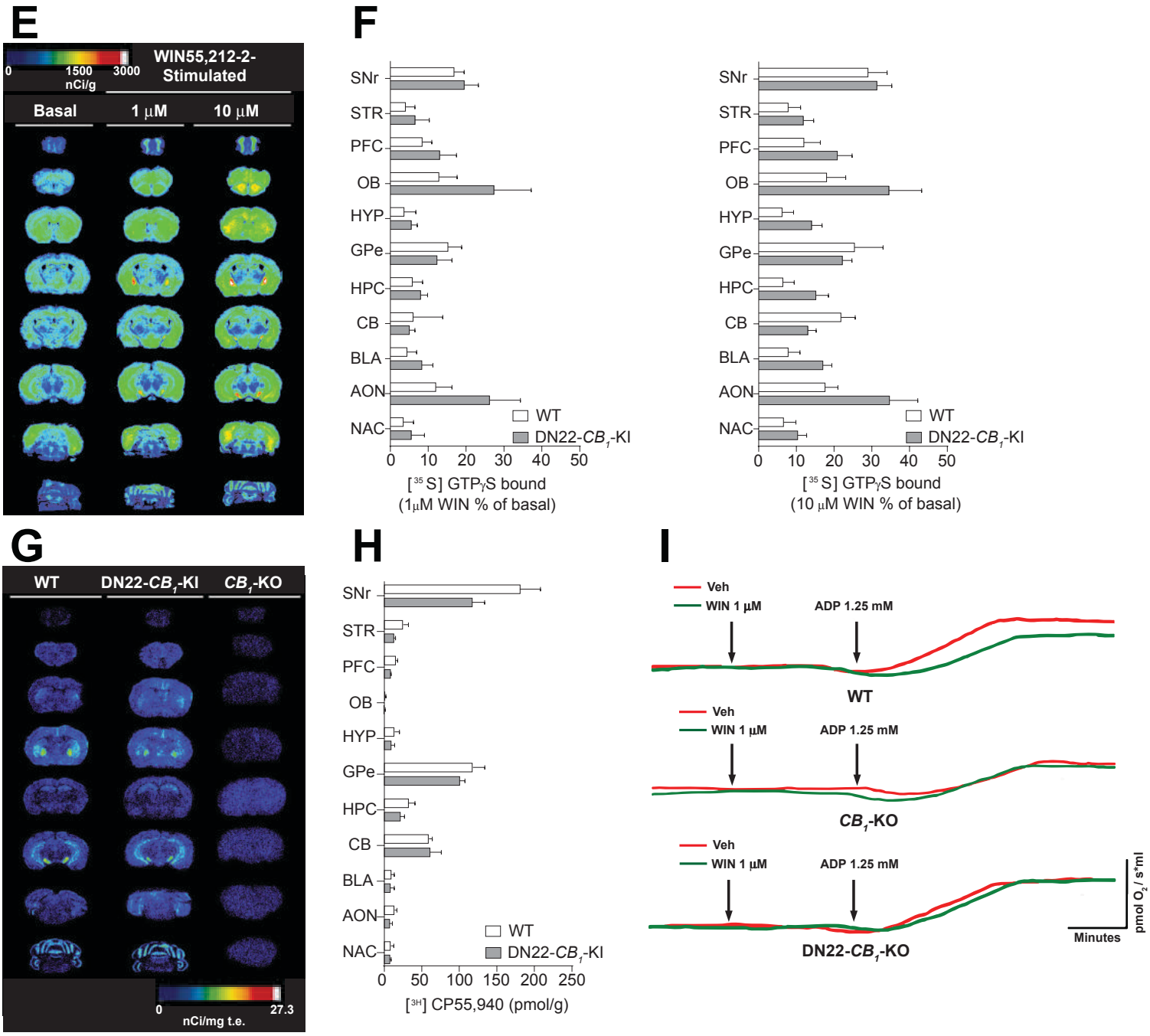

Figure S3

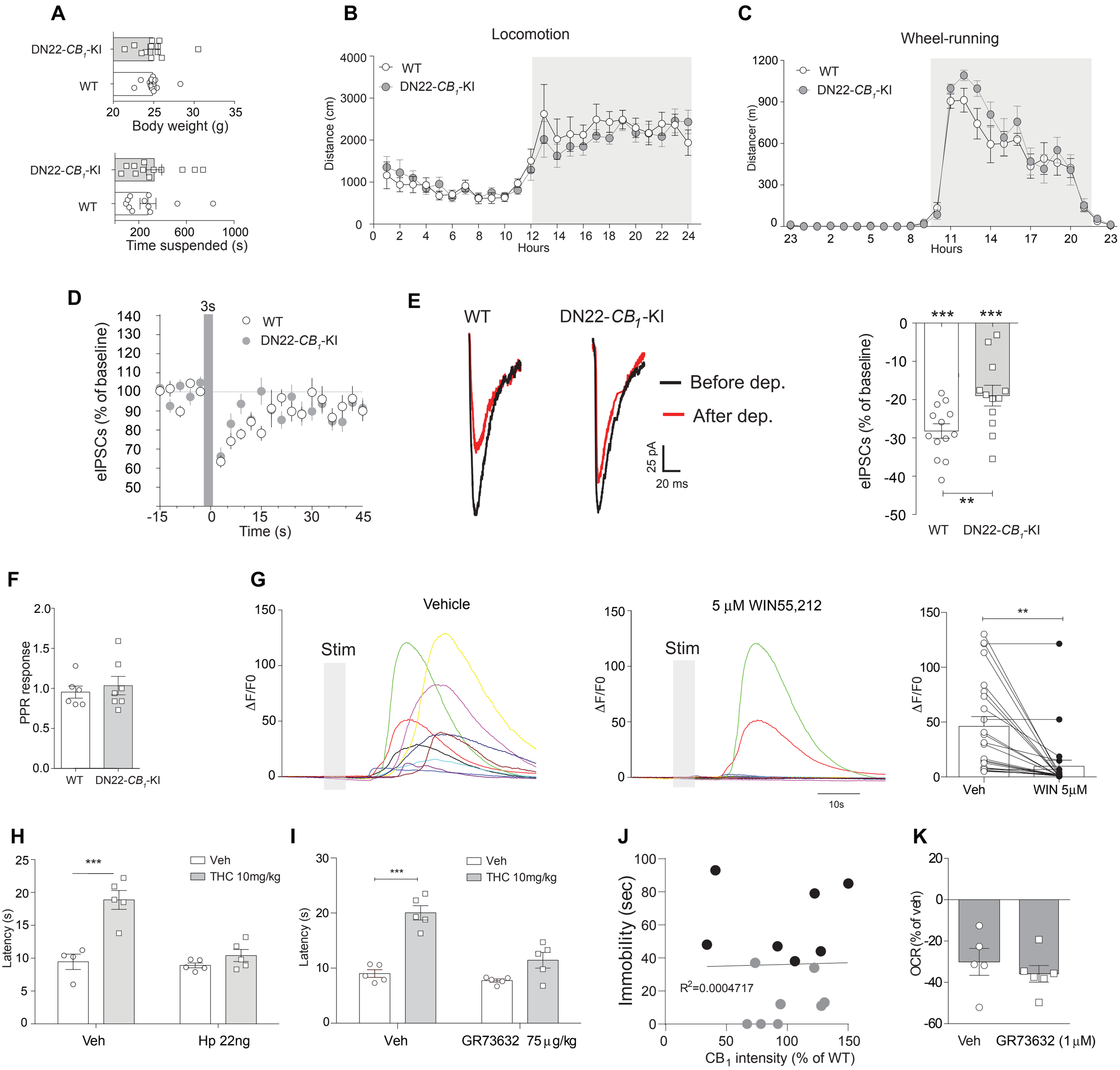
A
DN22-CB1-KI
WT
Body weight (g)
Time suspended (s)
B
Locomotion
WT
DN22-CB1-KI
Distance (cm)
Hours
C
Wheel-running
Distancer (m)
Hours
D
3s
eIPSCs (% of baseline)
Time (s)
E
WT
DN22-CB1-KI
Before dep.
After dep.
25 pA
20 ms
eIPSCs (% of baseline)
F
PPR response
G
Vehicle
5 μM WIN55,212
Stim
ΔF/F0
10s
Veh
WIN 5μM
H
Latency (s)
Veh
THC 10mg/kg
Hp 22ng
I
GR73632 75μg/kg
J
Immobility (sec)
R2=0.0004717
CB1 intensity (% of WT)
K
OCR (% of veh)
GR73632 (1μM)

Figure S3 (cont)

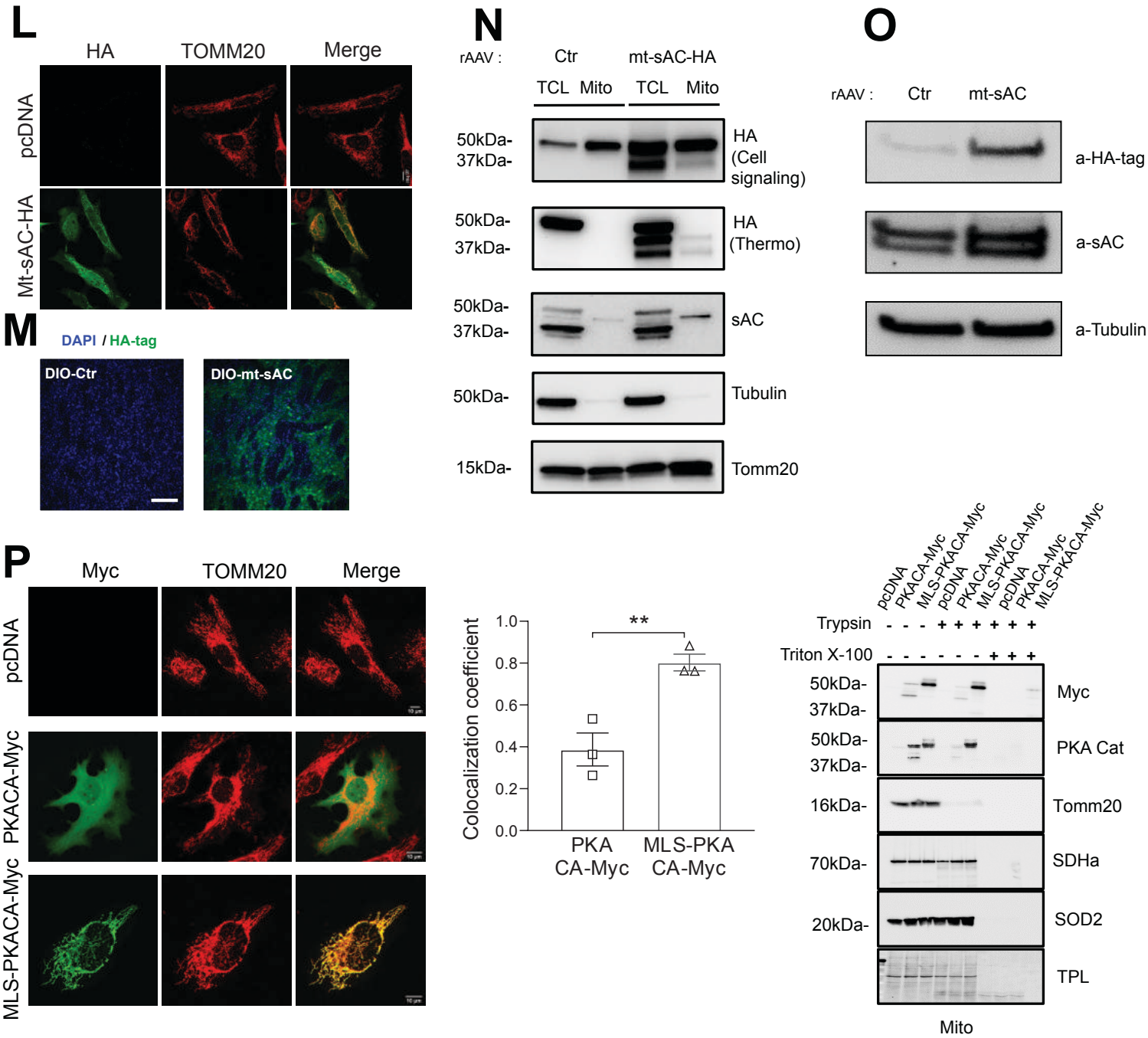

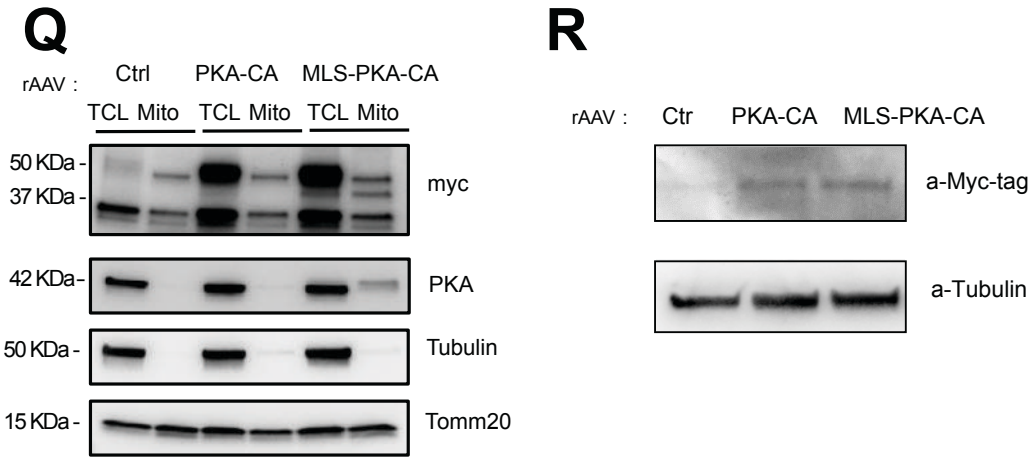

Figure S4

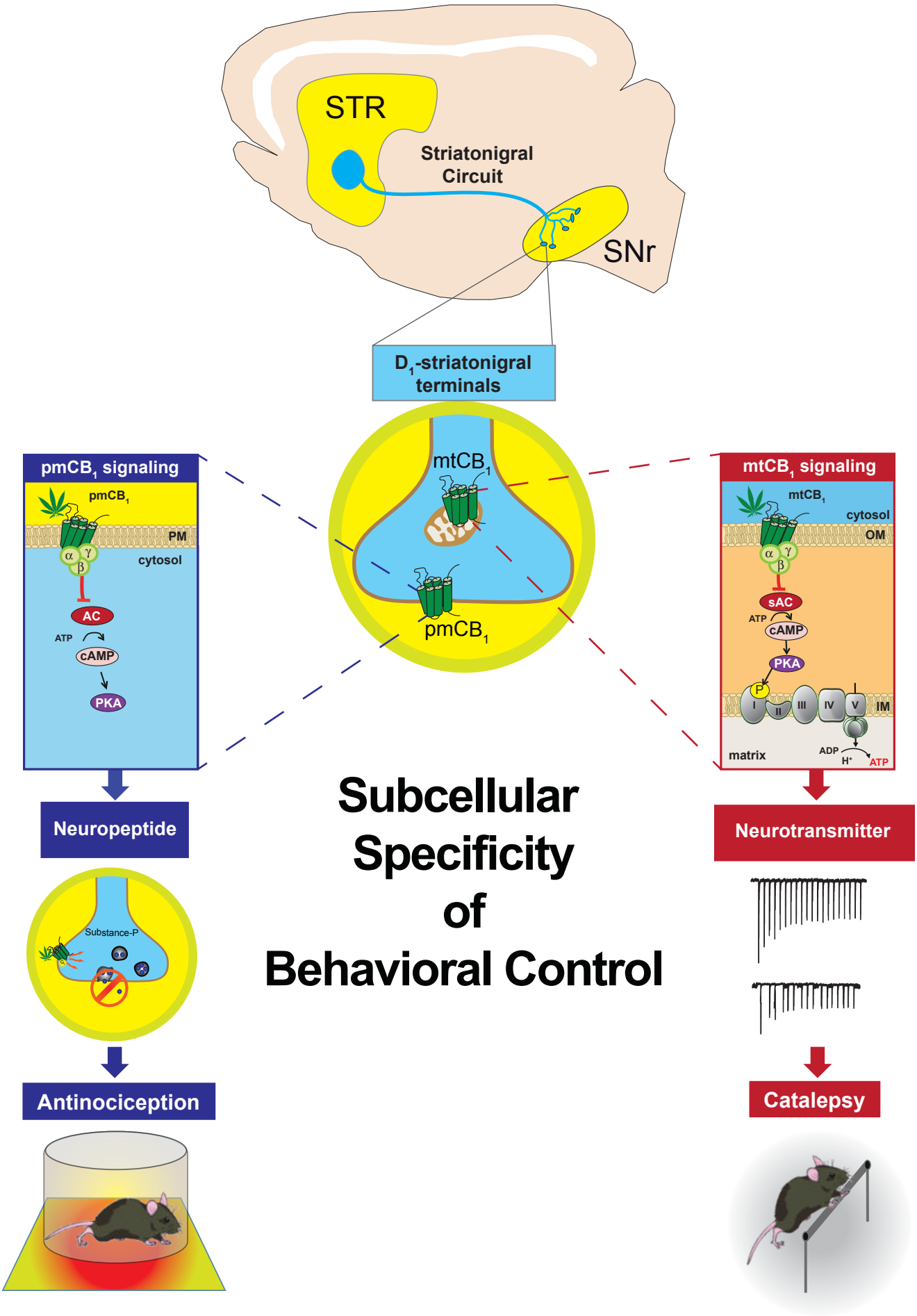

Subcellular Specificity of Behavioral Control